

2.09 Two-Dimensional Supramolecular Chemistry on Surfaces

C Pfeiffer and NR Champness, University of Nottingham, Nottingham, United Kingdom

© 2017 Elsevier Ltd. All rights reserved.

2.09.1	Introduction	181
2.09.2	Two-Dimensional Arrays Assembled Using Hydrogen Bonding	181
2.09.3	Two-Dimensional Arrays Assembled Using van der Waals Interactions	191
2.09.4	Covalently Coupled Two-Dimensional Arrays: Planar Covalent Organic Frameworks	191
2.09.5	Complex Structures With Low Degrees of Symmetry	192
2.09.6	Conclusions	197
References		198

2.09.1 Introduction

One key premise of supramolecular chemistry is the construction of nanoscale structures through the processes of self-assembly.¹ Self-assembly employs and exploits interactions between molecules such as hydrogen bonding and van der Waals interactions instead of covalent interactions within molecules. Using supramolecular interactions, highly complex molecular structures with targeted properties can be prepared without utilizing multistep synthetic pathways. Initially, solution-phase chemistry was the focus of supramolecular research.² More recently, developments have concentrated on solid-state chemistry in combination with crystal engineering.³ This shift of attention from solution-phase to solid-state structures is due to advances in characterization techniques that allow for precise identification of targeted supramolecular structures, in particular NMR and single crystal X-ray diffraction. Surface-based supramolecular structures have been recently explored and have led to an increased interest in fashioning low-dimensional, predominately two-dimensional, structures.^{4–10} Developments in surface-based supramolecular chemistry are the focus of this article. Emphasis will be on the synthetic approaches to such structures, particularly on the design of arrays through supramolecular interactions where molecules are specifically fashioned to control relative molecular organization. Hydrogen bonding to form extended arrays that propagate in two dimensions will be the focus of this article; however, other supramolecular interactions that will be highlighted include van der Waals interactions, metal–ligand coordination, and covalent coupling. Besides synthetic approaches, this article will discuss detailed characterization of the resulting two-dimensional arrays and the level of understanding that can be achieved using scanning probe microscopies, including scanning-tunnelling microscopy (STM) and atomic force microscopy (AFM).

Surface-based chemistry has long been used to assemble arrays of molecules. Perhaps the most widely studied area is the development of self-assembled monolayers (SAMs) of thiolate molecules adsorbed onto Au(111) substrates.¹¹ The simple deposition of molecules on surfaces, as seen with the Au–thiolate SAMs, leads to closed packed arrays with arrangements typically defined by van der Waals interactions and simple geometric formations. Combining this with supramolecular chemistry, more complex and potentially porous structures can be created by using intermolecular interactions, thus, logically expanding into the formation of robust covalently coupled arrays.

The surface used as the environment to assemble a given supramolecular array defines a two-dimensional boundary upon which the self-assembly process is developed. Suitable surfaces often studied include Au(111),¹² Ag–Si(111) $\sqrt{3} \times \sqrt{3}$ R30° [Ag/Si(111)],¹³ and highly oriented pyrolytic graphite (HOPG).¹⁴ However, recent studies have started to explore other substrates including graphene¹⁵ and boron-nitride (BN) monolayers.¹⁶ The choice of substrate is influenced by two factors: the tendency to adopt weak interactions with the molecules used in the self-assembly and the requirements of the scanning probe microscopy utilized. Noting the types of interactions involved in a system is significant in the choice of substrate. In the case of covalently coupled arrays, the surface can play an active role in promoting coupling reactions and therefore the choice of substrate is extremely important. In many instances, the determining feature has been dependent on the employed scanning probe microscopy. For instance, STM requires conducting surfaces in order to produce images; therefore, the choice of substrates is restricted to (semi)conducting materials. Recent improvements in resolution of AFM¹⁷ and the development of dynamic force microscopy (DFM)¹⁸ have led to a wider scope for characterization and expanded the selection of substrates to insulating materials.

This article is subdivided into four sections, systems assembled using (i) hydrogen bonds, (ii) van der Waals interactions, (iii) covalent bonds, and lastly a section (iv) on self-assembled systems with unusual ordering that illustrate the power of the approach and particularly the molecular-level characterization of such systems.

2.09.2 Two-Dimensional Arrays Assembled Using Hydrogen Bonding

The use of hydrogen bonds to create supramolecular structures goes back to the origins of the field.¹⁹ An early example of surface-based supramolecular chemistry is the formation of a unimolecular supramolecular structure mediated by hydrogen bonding reported by

Griessl et al.²⁰ The structure is prepared via deposition of trimesic acid onto an HOPG substrate in ultra high vacuum (UHV) conditions with subsequent imaging by STM, which reveals precise details of the self-assembled molecular structure. The intermolecular carboxylic acid:carboxylic acid hydrogen bonds, which adopt the classic, $R^2_2(8)$ intermolecular arrangement,²¹ ensure that an open structure is adopted in preference to any alternative close-packed arrangement. Importantly, this confirms that hydrogen-bonding interactions are the dominant force in determining the molecular arrangement of these structures. The observed structure is the expected honeycomb arrangement leading to a porous network structure; however, in addition to the honeycomb structure a secondary so-called “flower” arrangement is also observed by STM measurements. This alternative self-assembled structure results from the adoption of $R^3_3(12)$ supramolecular synthons formed by three carboxylic acid moieties from separate trimesic acid molecules. It is proposed that the “flower” structure forms due to a higher molecular density on the surface, indicating that surface coverage influences the final self-assembled structure, maximizing the energy gained through adsorbate–substrate interactions. Similarly, a study of an elongated analogue of trimesic acid, 1,3,5-tris(4-carboxyphenyl)benzene, also deposited on HOPG, but in this case from a range of alkyloic acids rather than by sublimation in UHV, also results in the formation of a honeycomb lattice at low temperatures, but a more densely packed phase at higher temperatures.²² The authors suggested that the coadsorption of solvent molecules within the honeycomb structure stabilizes the nominally porous structure at low temperatures, but upon elevation of the temperature the weakly bound solvent molecules desorb, initiating the transition to the more densely packed and thermodynamically favored phase.

A simple example of a unimolecular self-assembled structure that uses hydrogen bonds is that of naphthalene-1,4:5,8-tetracarboxylic diimide (NTCDI).²³ NTCDI contains imide moieties at opposing ends of the rod-shaped molecule which can adopt imide···imide hydrogen bonds. Analogous with carboxylic acid:carboxylic acid interactions an $R^2_2(8)$ intermolecular interaction is observed. As a result of the divergent arrangement of the imide moieties chains of molecules are observed when NTCDI is deposited onto a Ag/Si(111) surface (Fig. 1A). Imaging using DFM^{24–26} reveals submolecular details of the molecular arrangement. It is interesting to note that features in the DFM images appear to coincide with where hydrogen bonds would be expected to be observed (Fig. 1B); however, calculations indicate that these features do not arise as a result of the hydrogen bonds, but due to some other, as yet undefined, phenomenon. The origin of such intermolecular features remains a highly debated topic.²⁷

The full canvas of supramolecular design concepts can be brought to bear upon the construction of surface-based arrays and one area that has attracted considerable attention is the use of DNA nucleobases, which have specific hydrogen-bonding capability. The use of DNA nucleobases in supramolecular chemistry has been a persistent theme since the seminal work of Seeman²⁸ and has been developed by a number of research teams to significant effect²⁹ including some surface-based studies.^{30,31} In addition to the studies of self-assembly on surfaces of large DNA fragments, a particular focus for hydrogen-bonding studies has been the use of the

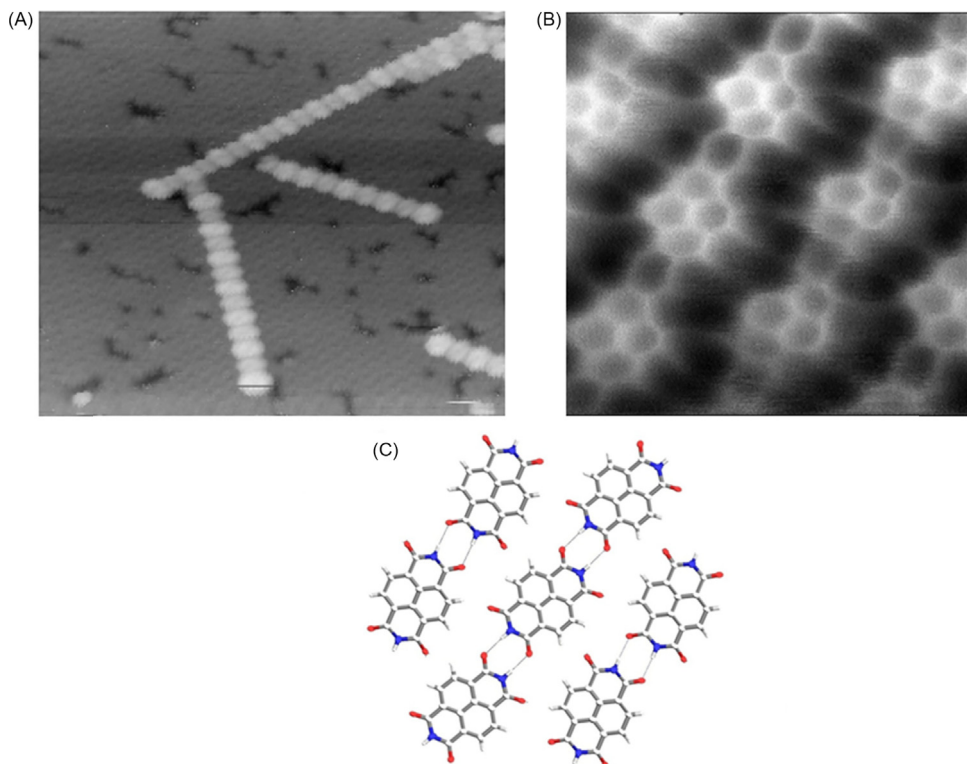


Figure 1 (A) STM image of three molecular chains of NTCDI adsorbed on Ag/Si(111)²³; (B) constant height DFM image of NTCDI adsorbed on Ag/Si(111) at 77 K (2.1×2.0 nm)²⁴; (C) view of hydrogen-bonded chains in the single crystal X-ray structure of NTCDI.²³ (A and C) Reproduced with permission from the American Chemical Society; (B) reproduced with permission from the Nature Publishing Group.

individual DNA bases to create self-assembled structures on surfaces. The assembly of guanine and its derivatives on surfaces has received particular attention.^{32–35} For example, the adsorption of guanine onto a Au(111) surface under UHV conditions leads to the formation of guanine quartets as imaged by STM.^{32,35} The quartets form through Hoogsteen-style hydrogen bonding and are associated through further N–H···N hydrogen bonds, leading to two-dimensional supramolecular arrays. This illustrates the complexity of using DNA bases due to the variety of potential hydrogen-bonding motifs that can be adopted from classic Watson–Crick pair formation, Hoogsteen interactions, reverse Watson–Crick, and reverse Hoogsteen arrangements (Fig. 2). Only the latest examples are highlighted here due to the area being reviewed only recently.³⁶

The hydrogen-bonding capability of DNA nucleobases can be exploited by attaching them as appendages to more complex molecules, potentially leading to enhanced control over supramolecular structure. An example of such a strategy is given by the study of a porphyrin molecule (tetra-TP) in which the porphyrin core is functionalized in each meso-position by a phenylthymine moiety such that each thymine presents a hydrogen-bonding face *exo* to the porphyrin core.³⁷ The molecule self-assembles on an HOPG substrate to give rise to a two-dimensional structure wherein the molecules interact through R²(8) intermolecular thymine···thymine hydrogen bonds (Fig. 3A). The asymmetric arrangement of the thymine groups appended to the tetra-TP molecules suggests the potential for the molecules to adopt a chiral arrangement when adsorbed onto a surface and this is indeed observed. The almost perfectly square two-dimensional unit cell observed for the tetra-TP structure suggests that all of the thymine groups within an individual tetra-TP molecule adopt the same orientation with respect to the porphyrin, and that individual domains contain only molecules of the same handedness. Overall the array of tetra-TP remains globally achiral by forming an equal area of domains containing either right- or left-handed molecules. The formation, by prochiral molecules, of homochiral domains on surfaces containing molecules of only a single handedness has been noted in many previous studies.³⁸ Addition of a substituted adenine species, 9-propyladenine, to the assembly of tetra-TP produces a molecular network with a combination of disordered regions interspersed with small domains of an ordered cocrystal structure containing both tetra-TP and 9-propyladenine. As anticipated, favorable Watson–Crick thymine–adenine interactions are observed, but interestingly dimers of adenine are also formed. They achieve a high surface coverage and form an additional N–H···N hydrogen bond to a further tetra-TP molecule (Fig. 3B). The complexity of the structure reveals the difficulties in designing such structures, even when relatively predictable hydrogen-bonding synthons are present.

A related approach has been used by González-Rodríguez and De Feyter³⁹ who designed rod-shaped molecules decorated by DNA bases at the molecule's termini, either with guanine (G) and cytosine (C) or adenine (A) and uracil (U) (Fig. 4A). The rods are designed such that opposing ends will form complementary hydrogen-bonding groups. Additionally, the authors functionalized the rods with alkyl tails such that any residual space in the structure could be occupied such that no additional molecules are required to fill space within the structure. Self-assembly on a HOPG substrate results in the formation of cyclic structures, as confirmed by STM imaging (Fig. 4B), indicating the successful employment of the complementary hydrogen-bonding moieties in forming heteromolecular hydrogen-bonding interactions (G:C or A:U). Despite the alkyl chain appendages filling the space within the cyclic structures, the GC system is capable of adsorbing coronene with the alkyl chains assumed to vacate the space due to preferential physisorption of the large, flat, polyaromatic guest onto the HOPG surface.

Moving beyond DNA systems it is possible to create nonnatural, hydrogen-bonding synthons for the generation of extended two-dimensional arrays. For example, the triple hydrogen-bonding interaction between 2,6-di(acetylamino)pyridines and imide groups has received extensive study in supramolecular chemistry^{19,40} and can also be exploited to form bimolecular structures on surfaces.⁴¹ An early example of a bimolecular network was prepared from perylene-3,4,9,10-tetracarboxylic diimide (PTCDI), which bears two imide appendages at opposing ends of the rod, similar to NTCDI discussed above, and melamine (Fig. 5).⁴²

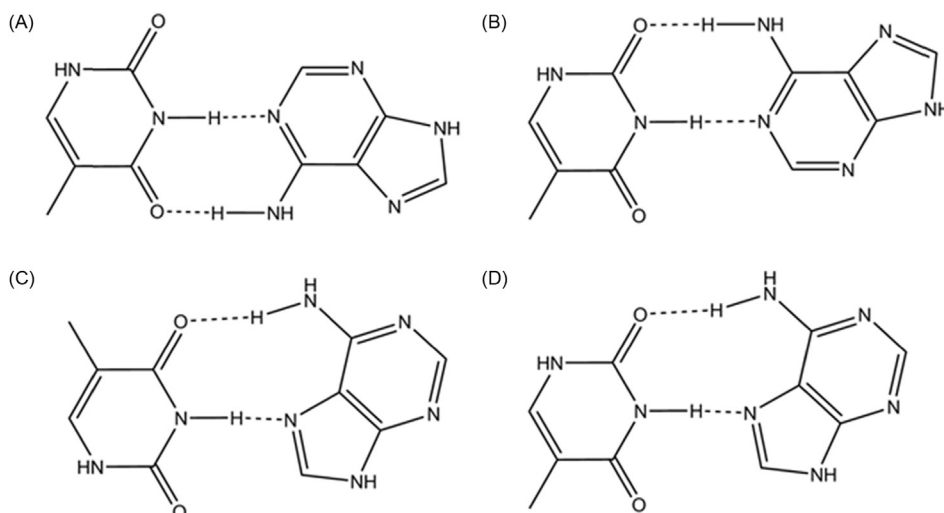


Figure 2 Potential hydrogen-bonding interactions between thymine and adenine: (A) standard Watson–Crick, (B) reverse Watson–Crick, (C) Hoogsteen, and (D) reverse Hoogsteen arrangements.

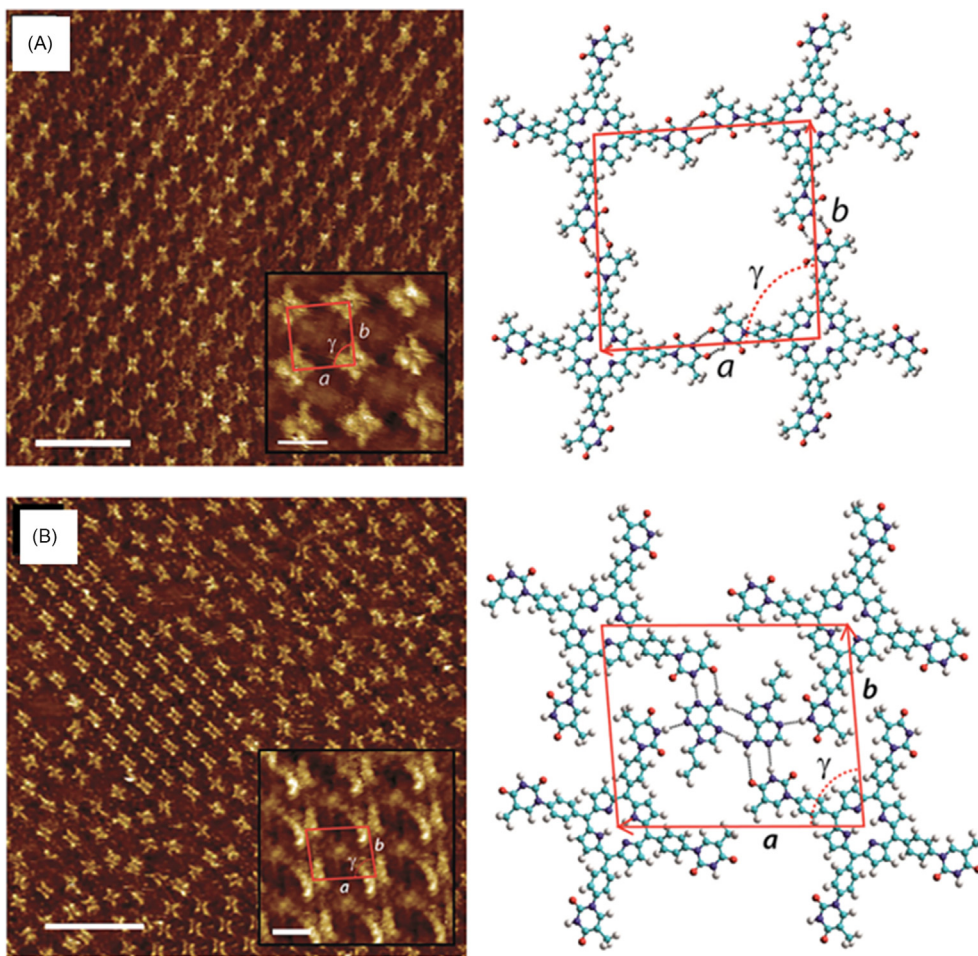


Figure 3 (A) Two-dimensional self-assembled network of tetra-TP adsorbed on HOPG liquid–solid interface, left: STM image. The inset shows a high resolution, drift corrected STM image of the network with an individual 2D unit cell marked in red; scale bar = 20 nm (inset = 2 nm). Right: Molecular model of the tetra-T-porphyrin network from molecular mechanics (MM) simulations. (B) 2D self-assembled network of tetra-TP and 9-propyladenine adsorbed on HOPG liquid–solid interface, left: STM image. The inset shows a high resolution, drift corrected STM image of the network with an individual 2D unit cell marked in red; scale bar = 20 nm (inset = 1.6 nm). Right: Molecular model of the tetra-T-porphyrin/9-propyladenine network from MM simulations.³⁷ Reproduced with permission from the Royal Society of Chemistry.

Codeposition of the two building blocks onto a Ag/Si(111) surface under UHV conditions results in the formation of a honeycomb network with triple hydrogen bonds formed between the PTCDI imide moieties and each side of the triangular melamine molecule. The network was found to be commensurate with the underlying Ag/Si(111) surface, indicating an influence from the substrate in the formation of the network.

Large pores are formed by the network, with a diameter of 2.4 nm, which are capable of hosting several large molecules as initially demonstrated by the encapsulation of C₆₀⁴² (Fig. 5). The entrapment of C₆₀ by the PTCDI–melamine hexagonal network leads to the formation of heptamic C₆₀ clusters within the pores. The arrangement and properties of the C₆₀ clusters were found to differ from close-packed fullerene on the same surface, which in contrast to the heptamers does not align with the principle axes of the underlying Ag/Si(111) substrate, thus demonstrating the templating and stabilizing effects of the network.⁴² Indeed, the ability of the PTCDI–melamine family of arrays has been shown to host other fullerenes including C₈₄⁴³ and Lu@C₈₂,⁴⁴ and a range of molecules discussed in more detail later.

The PTCDI–melamine network⁴² can also be prepared on a Au(111) surface,⁴⁵ leading to an analogous honeycomb arrangement to that observed on a Ag/Si(111) substrate. However, after annealing at higher temperatures, a parallelogram phase was also observed on Au(111), which has the same stoichiometric ratio as the honeycomb structure, but is more dense.⁴⁶ The parallelogram phase is also capable of trapping guest molecules such as C₆₀, but due to the restricted cavity size only two C₆₀ molecules are hosted, the size of the cluster being defined by the physical size of the network pores. Similar studies have demonstrated the entrapment of Lu@C₈₂ by the parallelogram phase, but in this case only single fullerenes are accommodated within each pore.⁴⁴ The parallelogram PTCDI–melamine phase is also able to trap two decanethiol molecules which sit parallel to the surface under the UHV conditions used. The entrapment of a potentially more reactive molecule, such as a thiol, confirms that such networks

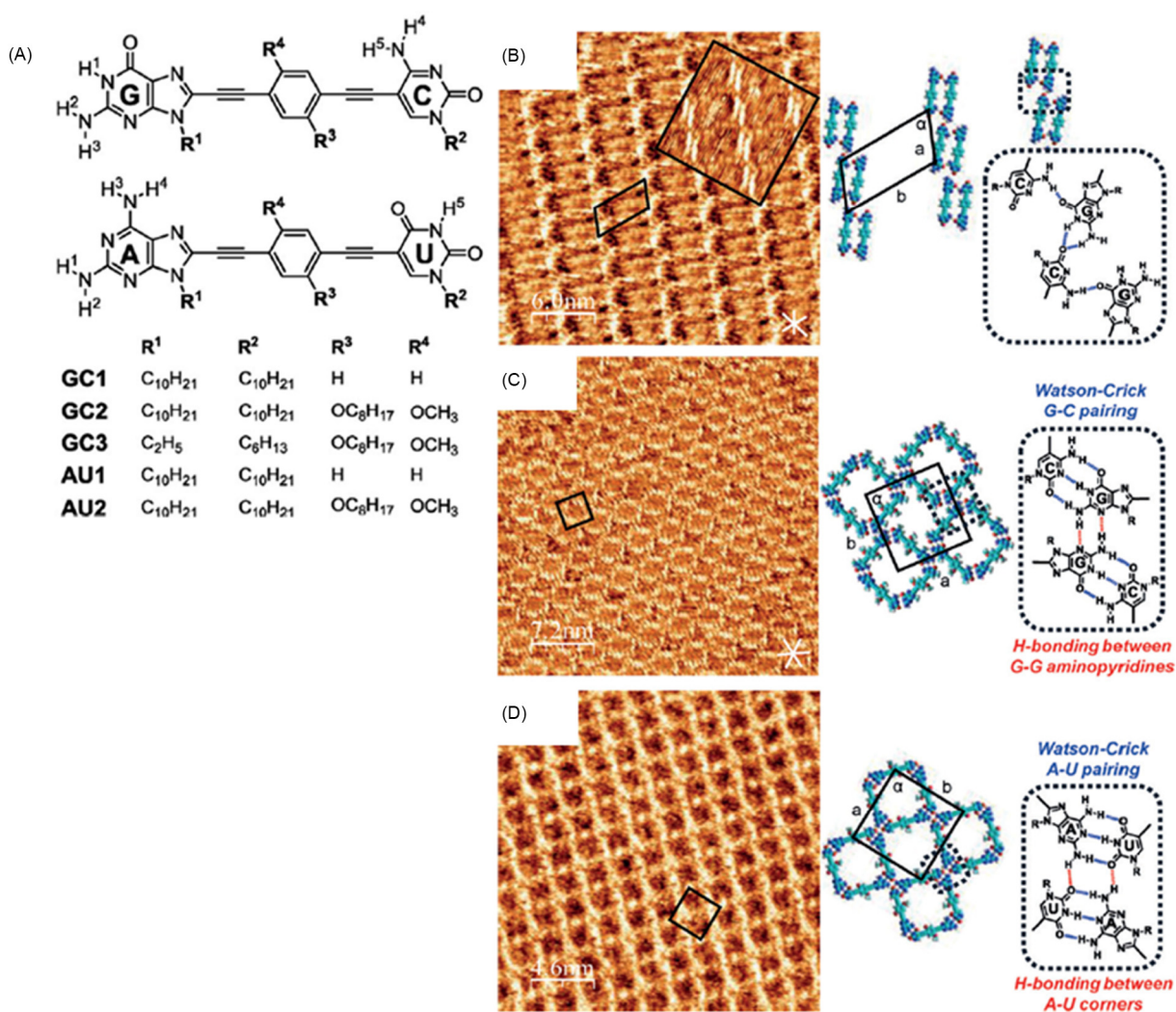


Figure 4 (A) Mixed guanine–cytosine and adenine–uracil hydrogen-bonding rods employed for self-assembly.³⁹ (B) STM image of GC1 on HOPG showing pairs of monomers and model of observed structure. (C) STM image of GC2 on HOPG and model of observed cyclic structure. (D) STM image of AU2 on HOPG and model of observed cyclic structure.³⁹ Reproduced with permission from Wiley-VCH Verlag GmbH and Co. KGaA.

have the potential for trapping a range of different species. It is interesting to note that adsorption of decanethiol onto the PTCI-melamine arrays, in UHV, leads to the destruction of the honeycomb phase, but not the parallelogram phase, suggesting that the latter is preferentially stabilized by the thiol guest.⁴⁷

The adsorption of thiol guests within the pores of PTCI-melamine networks has been advanced significantly by Buck et al.^{48,49} It has been demonstrated that the PTCI-melamine network can be assembled on a Au(111) surface from solution and used for a variety of applications, particularly as a patterning tool (Fig. 6).^{48,49} Due to the solution-based preparative procedure it is possible to apply traditional Au-thiolate SAM-synthesis. The adsorption of adamantanethiol within the pores of the network is demonstrated with the thiolates sitting perpendicular to the surface, in contrast to related studies in UHV conditions.⁴⁷ The clusters of adsorbed thiols, or confined SAMs, in this example confirmed that adamantanethiol SAMs can be exploited to guide the deposition of copper atoms within the pores using underpotential deposition. Copper metal was successfully deposited only on areas of the surface that were not covered by the network, that is, those areas covered by thiols⁴⁸ and a subsequent study demonstrated that the PTCI-melamine network acts as a diffusion barrier for copper atoms.^{49,50}

The encapsulation of thiol-decorated molecules by the PTCI-melamine network has been exploited further with examples that demonstrate the versatility of the approach. Such studies have included the entrapment of thiol-functionalized porphyrins⁵¹ and complex functionalized polyoxometalates (POM).⁵² The latter study reports the entrapment of a disulfide-functionalized Keggin-type POM, [PW₁₁O₃₉Ge-*{p*-C₆H₄-CC-C₆H₄-NHC(O)(CH₂)₄{-CH(CH₂)₂S-S-} }]⁴⁻, into the PTCI-melamine array which has been adsorbed on a Au(111) substrate. Through formation of a Au–S bond the functionalized POM can be trapped specifically within the pores of the self-assembled array. STM studies indicate spatial resolution of the POMs that is reminiscent of the underlying supramolecular array (Fig. 7).

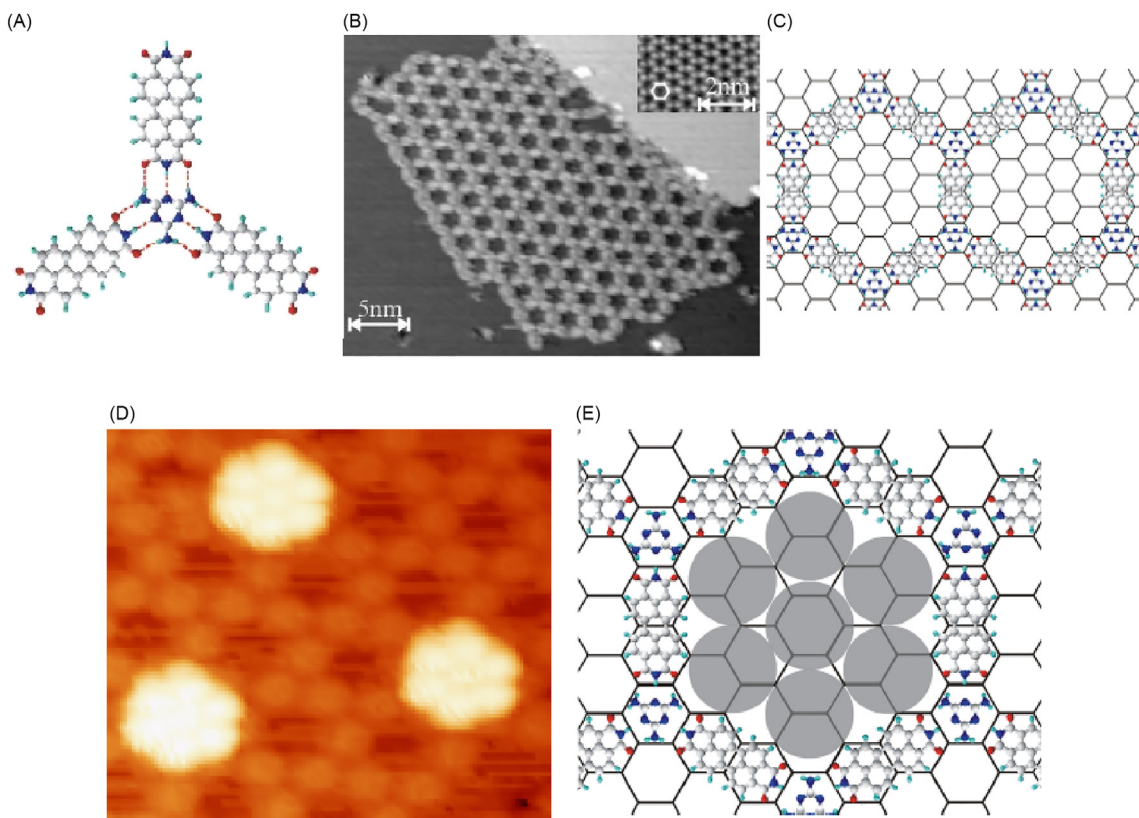


Figure 5 (A) Schematic of the PTCDI–melamine junction, showing the nine hydrogen bonds that make up the structural node as dashed red lines. (B) STM image of the PTCDI–melamine network on Ag/Si(111); inset, high resolution view of the Ag/Si(111) surface. (C) Schematic of the network showing the registry with the hexagonal substrate. (D) STM image of fullerenes trapped within the pores of the hexagonal network, seen as bright white features. (E) Schematic diagram of a C_{60} heptamer sitting within a pore.⁴² Reproduced with permission from the Nature Publishing Group.

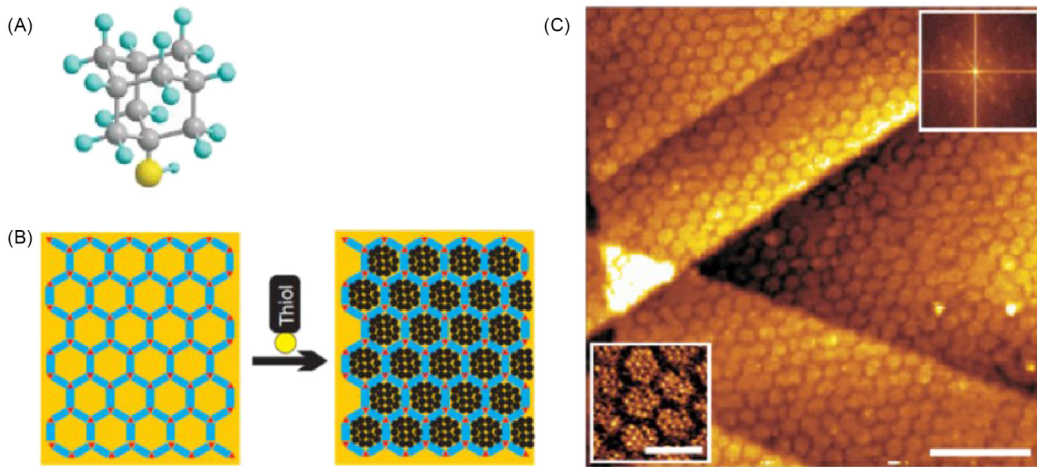


Figure 6 (A) The adamantanethiol molecule. (B) Schematic of the network filling process. (C) STM image of the PTCDI–melamine network on Au(111)/mica filled with adamantanethiol, scale bar = 20 nm. Insets: higher resolution STM image and Fourier transforms, scale bar = 5 nm.⁴⁸ Reproduced with permission from the Nature Publishing Group.

Sublimation or solution-phase deposition can be employed to adsorb molecules onto hydrogen-bonded arrays but these techniques are not always suitable for sensitive molecules and thus a further technique has been developed using electrospray deposition.^{53,54} Electrospray techniques have been used to deposit $Mn_{12}O_{12}(O_2CCH_3)_{16}(H_2O)_4$ clusters, a molecule of interest due to its ability to act as a single molecule magnet, onto the PTCDI–melamine array on a Au(111) substrate.⁵⁴ The softer deposition

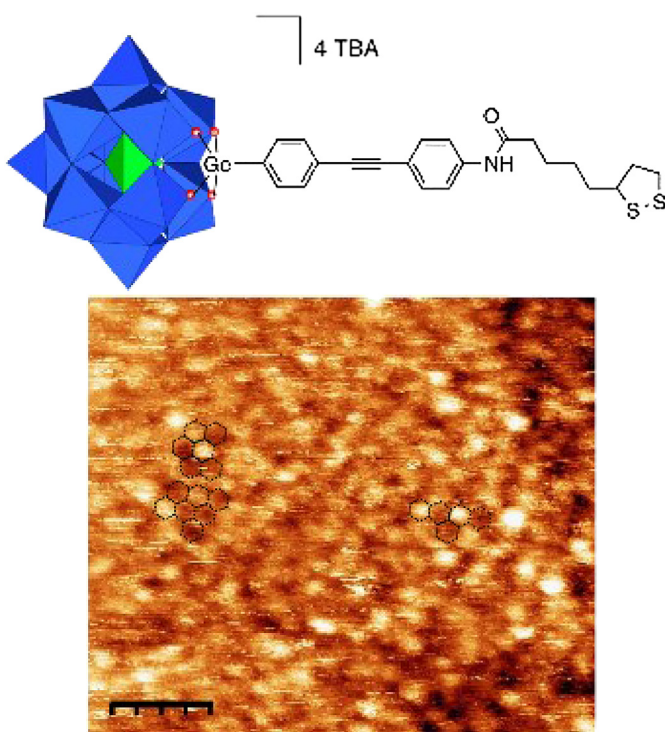


Figure 7 A disulfide-functionalized POM (shown above with blue WO_6 octahedra depicted with oxygen atoms at the vertices and metal cations buried inside) and a STM image showing the POM trapped within the PTCDI–melamine network on a Au(111) substrate. POMs can be seen as *bright white features* and the PTCDI–melamine array is indicated by the *black dotted lines*, scale bar = 16 nm.⁵² Reproduced with permission from the American Chemical Society.

technique is required as sublimation is not possible for $\text{Mn}_{12}\text{O}_{12}(\text{O}_2\text{CCH}_3)_{16}(\text{H}_2\text{O})_4$ due to its decomposition at elevated temperatures. In the absence of the hydrogen-bonded array the $\text{Mn}_{12}\text{O}_{12}(\text{O}_2\text{CCH}_3)_{16}(\text{H}_2\text{O})_4$ clusters assemble generating filamentary structures on the surface (Fig. 8B). In contrast adsorption of $\text{Mn}_{12}\text{O}_{12}(\text{O}_2\text{CCH}_3)_{16}(\text{H}_2\text{O})_4$ clusters onto the PTCDI–melamine array results in a low degree of ordering with some molecules accommodated within the pores of the network but with others positioned on top of the array (Fig. 8C). The entrapment of the $\text{Mn}_{12}\text{O}_{12}(\text{O}_2\text{CCH}_3)_{16}(\text{H}_2\text{O})_4$ clusters in the array is not as efficient as that of other species, including fullerenes, most probably due to a mismatch of dimensions between the cluster (1.6 nm) and pore (2.5 nm). This study indicates that maximum organization of guest molecules by porous frameworks can be achieved by idealizing size match between host and guest and by maximizing interactions between host and guest.

An advantage of the bimolecular approach to array formation is that each component can be altered, allowing for modification of the resulting structure. Thus, for the PTCDI–melamine arrays the PTCDI molecule^{56,57} can be readily functionalized, leading to manipulation of the framework and cavity dimensions within the array. Importantly, modification of the components not only affects the sterics and dimensions of the building blocks, but can also affect their physical and chemical properties and tune their solubility for studies at the surface–solution interface. By introducing steric bulk to the PTCDI molecules, the available space for guest entrapment can be controlled which results in networks that can potentially trap individual molecules in a regular array. Self-assembled arrays formed between melamine and PTCDI derivatives, and in some examples networks formed by the functionalized PTCDI derivatives alone, are able to act as hosts to guest molecules.^{56,57} For example, self-assembly of thioadamantyl functionalized PTCDI, (SAdam)₂-PTCDI, and melamine leads to the anticipated honeycomb array.⁵⁷ The thioadamantyl groups are both bulky and rigid and therefore would be expected to provide an effective mechanism for inhibiting the space within the network pores. However, upon formation of a (SAdam)₂-PTCDI–melamine network some of the thioadamantyl groups are cleaved from the PTCDI moieties.⁵⁷ Consequently, a variety of distinct pore sizes and configurations are formed which can be visualized following C_{60} adsorption onto the network and subsequent STM imaging. Individual C_{60} molecules are more readily imaged by STM than the underlying thioadamantyl groups and, by employing this approach, it is feasible to identify the different orientations of the molecular clusters within each pore. The number of C_{60} molecules adsorbed within a given pore is determined by the degree of thioadamantyl cleavage and clusters ranging from dimers to heptamers are observed. Considering the dimensions of the honeycomb pores and the size of the thioadamantyl appendages, clusters of greater than five fullerenes can only be explained by cleavage of the thioadamantyl groups, the heptamers corresponding to a pore where no thioadamantyl appendages remain. Further constriction of pore size can be used to control the number of guest molecules, a principle demonstrated by the array formed by 1,7-bis(4-benzoic acid)-3,4,9,10-perylenetetracarboxylic diimide.⁵⁸ As with many disubstituted PTCDI species,⁴¹ Bz₂-PTCDI assembles into a unimolecular honeycomb array, without the need to add melamine, through the adoption of a tri-molecular $\text{R}_3(12)$

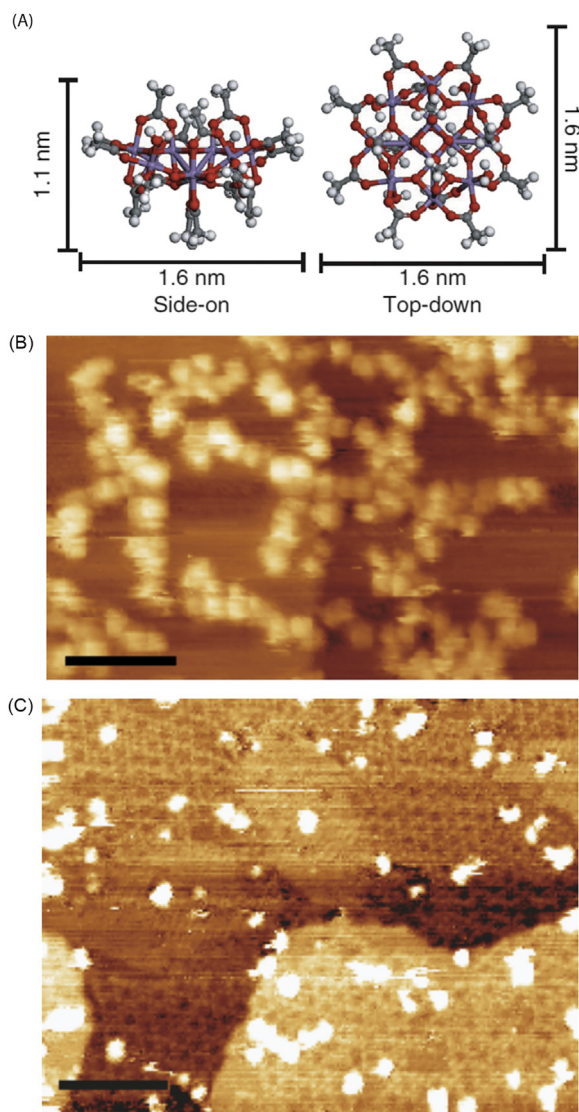


Figure 8 (A) Schematic representation of $\text{Mn}_{12}\text{O}_{12}(\text{O}_2\text{CCH}_3)_{16}(\text{H}_2\text{O})_4$; STM images showing (B) the filamentary structures formed by molecular aggregates comprised of individual $\text{Mn}_{12}\text{O}_{12}(\text{O}_2\text{CCH}_3)_{16}(\text{H}_2\text{O})_4$ molecules, scale bar = 10 nm. (C) $\text{Mn}_{12}\text{O}_{12}(\text{O}_2\text{CCH}_3)_{16}(\text{H}_2\text{O})_4$ molecules deposited onto a PTCDI–melamine network on a Au(111) surface, scale bar = 20 nm.⁵⁴ Reproduced with permission from the Nature Publishing Group.

hydrogen-bonded junction (see the succeeding text). The rigid protrusion of the phenylcarboxylate moieties into the framework cavities leads to the encapsulation of single C_{60} molecules within each pore, which are in turn spaced in a regular fashion across the surface.

The material employed as substrate for the self-assembly process clearly influences the self-assembly process and the resulting framework structure and should not be considered an innocent agent in the synthetic strategy. The influence that the substrate can have on supramolecular assembly is illustrated by the use of graphene or boron-nitride (BN) “nanomesh” monolayers grown on Rh(111) crystals.⁵⁵ Both systems exhibit moiré patterns that introduce distinct adsorption sites on the surface. The self-assembly of PTCDI and related di-functionalized derivatives, 1,7-dipropylthio-perylene-3,4:9,10-tetracarboxydiimide (DP-PTCDI) and 1,7-di(butyl)-coronene-3,4:9,10-tetracarboxylic acid bisimide (DB-CTCDI), on graphene has been studied by STM (Fig. 9).⁵⁵ Two distinct junctions formed by either two or three molecules are observed and result in different assemblies (Fig. 9C, 9D). For example, unfunctionalized PTCDI forms rows up to 25 nm in length running parallel to the principal directions of the substrate and adopts only simple dimeric hydrogen-bonding arrangements. The molecular arrangement on the graphene superstructure differs significantly from that observed for a graphite substrate, on which three-dimensional islands are formed.⁶⁰ The importance of a commensurate match between molecular dimensions and the moiré periodicity is demonstrated by a comparison with adsorption of PTCDI on a BN “nanomesh” monolayer (Fig. 9). The BN monolayer is isoelectronic with graphene but has a slightly larger periodicity of 3.2 nm, which is noncommensurate with the dimensions of PTCDI. On BN [on Rh(111)], individually isolated PTCDI molecules are trapped in energy minima associated with the moiré pattern which clearly demonstrates the influence of

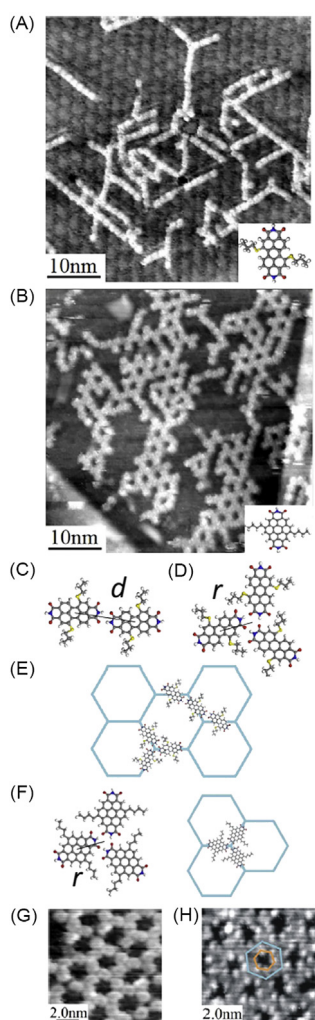


Figure 9 STM images acquired following deposition of (A) DP-PTCDI, (B) DB-CTCDI on a graphene monolayer formed on Rh(111). (C and D) Diagram of junctions between DP-PTCDI dimers (C) and trimers (D) stabilized, respectively, by two and three C=O \cdots NH hydrogen bonds between neighboring molecules with dimer center–center spacing of d and trimer vertex to molecule center spacing r . (E) Placement of DP-PTCDI trimers and dimers. (F) DB-CTCDI trimer junction analogous to (D) with vertex to molecule center spacing r and placement of DB-CTCDI trimer on the graphene superstructure. (G and H) STM images of DB-CTCDI showing chirality of junctions and intramolecular details of molecules. The hexagons in (H) highlight the chirality of the molecular arrangement.⁵⁵ Reproduced with permission from Wiley-VCH Verlag GmbH and Co. KGaA.

the underlying substrate on supramolecular assembly. On graphene both DP-PTCDI and DB-CTCDI form linear rows that are built using dimeric hydrogen bond junctions, and more complex arrays which include junctions where three molecules meet in a hydrogen-bonded trimeric arrangement. In the case of DP-PTCDI the ratio of dimer:trimer junctions is 75:25 in comparison to less than 1% of junctions being trimers for unfunctionalized PTCDI. In the case of DB-CTCDI the three molecule junctions dominate the self-assembly process, with no linear dimers unambiguously identified. The array constructed from trimeric junctions results in a honeycomb framework aligned with the graphene monolayer superstructure and encloses the areas of bright contrast arising from the moiré pattern.

The intermolecular hydrogen-bonding synthon exploited in the PTCDI-melamine arrays can be readily incorporated into other building blocks (e.g., thymine includes the same imide moiety seen in PTCDI) and thus many possible arrays can be targeted. Perhaps the simplest example is the self-assembled array formed between cyanuric acid and melamine.^{61,62} Samori et al.⁶³ have elegantly demonstrated the self-assembly of a range of diimide molecules and melamine (Fig. 10) at the solution/solid interface on an HOPG surface following deposition from a 1,2,4-trichlorobenzene/dimethylsulfoxide solution. The formation of hexagonal/honeycomb networks is anticipated for such systems in an analogous fashion to the PTCDI-melamine systems, and such arrays are observed, but detailed studies of concentration variation lead to the adoption of a range of structures. The nature of the structures formed by combinations of the diimide molecules (labelled 1–4 in Fig. 10) with melamine ranges from open hexagonal networks to close-packed structures and significantly varies with component concentration. Ultimately, a phase diagram of polymorphs is generated for these systems which gives perspective to the complexity of the self-assembly processes involved (Fig. 10).

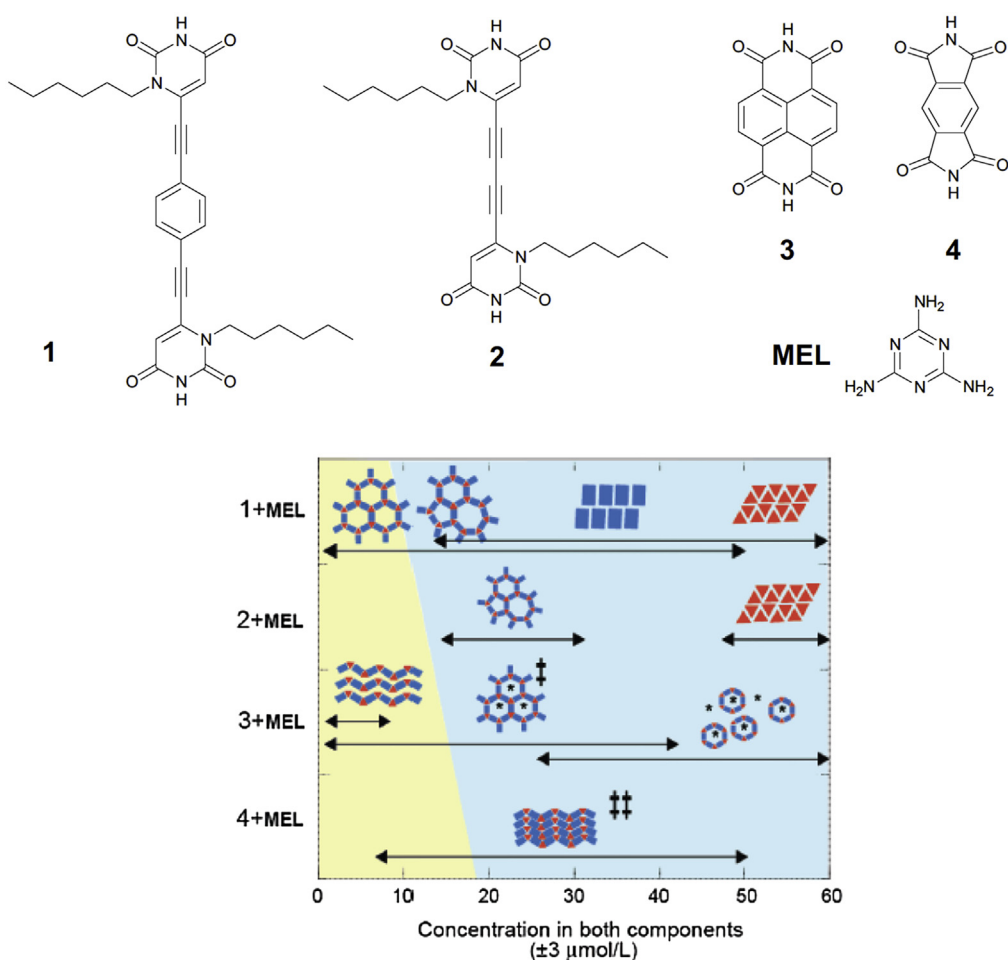


Figure 10 Diimide molecules used by Samori et al.⁶³ in combination with melamine (MEL) to afford self-assembled structures (top). The nature of the structure is concentration dependent giving rise to a range of polymorphic products (bottom). Reproduced with permission from the American Chemical Society.

Elongated analogues of PTCDI have also been employed in the synthesis of supramolecular arrays in combination with melamine. In particular, a functionalized terrylene diimide has been used to assemble a honeycomb network, analogous to the PTCDI–melamine array discussed in the preceding text.⁶⁴ The terrylene diimide–melamine array is assembled on a graphene passivated diamond (Fig. 11) and by using a gallium drop as a counter electrode the photocurrent of the array can be measured. It was found that under irradiation at 710 nm an incident photon to current efficiency of 0.6% was observed. The study indicates the possible application of such self-assembled supramolecular arrays for the fabrication of optoelectronic devices.

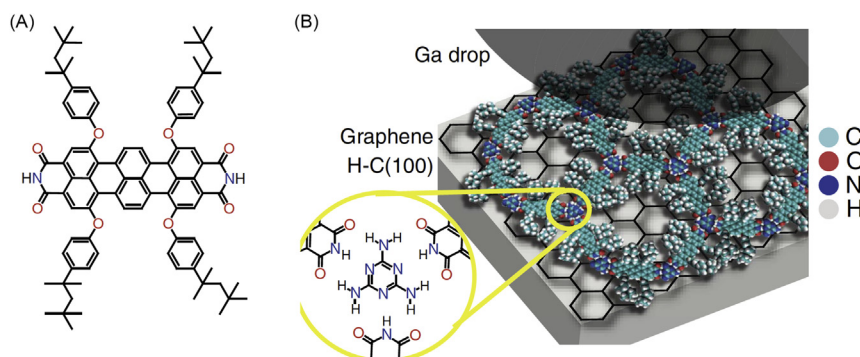


Figure 11 (A) Functionalized terrylene diimide employed in the assembly of (B) a terrylene diimide–melamine array on a graphene passivated diamond surface. A gallium drop is used as a counter electrode to study the photoresponse of the supramolecular array.⁶⁴ Reproduced with permission from the Nature Publishing Group.

2.09.3 Two-Dimensional Arrays Assembled Using van der Waals Interactions

The role of van der Waals interactions in the creation of surface supramolecular frameworks cannot be underestimated. A large number of studies have been reported using van der Waals interactions to create supramolecular structures and these have been reviewed on a number of occasions.^{7–9,65,66} A particularly notable interaction that has been widely exploited is the strong adsorption between alkyl chains and HOPG. The role of the alkyl chain is clearly significant in the resulting assembly process, and interdigitation of alkyl chains from adjacent molecules is commonly observed and provides a method of control over the molecular arrangement. A representative example of a self-assembled framework controlled by van der Waals interactions was investigated by Schull et al.⁶⁷ 1,3,5-tris[(E)-2-(3,5-didecyloxyphenyl)-ethenyl]-benzene, a trimeric compound with six pendent decyl chains, was deposited onto an HOPG substrate. Self-assembly through interdigitation of the alkyl chains causes the formation of a porous network within which coronene and hexabenzocoronene could be accommodated. The coadsorption of coronene or hexabenzocoronene modified the nature of the resulting structure, in a similar fashion to solution-phase host–guest chemistry. Indeed, interdigitation of alkyl chains has been extensively used by De Feyter and coworkers in a number of elegant studies.^{7–9,65,66,68–73} One area of particular focus of research has been the study of alkoxylated dehydrobenzo[12]annulenes.⁶⁸ A representative study of rhombic-shaped dehydrobenzo[12]annulenes assembled at a 1,2,4-trichlorobenzene/HOPG interface⁶⁸ demonstrates that variation in the chain length of alkyl substituents results in five distinct network structures, three porous and two nonporous structures.⁶⁸ Shorter alkyl chain substituents on the dehydrobenzo[12]annulene core favor formation of porous frameworks, whereas those with longer alkyl chains tend towards the formation of nonporous arrangements. Concentration of the building blocks in solution also plays a key role in the nature of the structures formed. Dilution of the dehydrobenzo[12]annulenes solutions leads to the transformation of nonporous structures into porous frameworks as a result of factors related to overall surface coverage.

As in the solid state, the subtle interplay of different intermolecular supramolecular interactions can lead to the formation of a range of different structures with little energetic differences between the different arrangements, that is, polymorphs. A study by De Feyter⁵⁹ describes an approach to establish the range of polymorphs for a given system using building blocks that exploit van der Waals interactions or hydrogen-bonding interactions. The formation of polymorphs in two-dimensional supramolecular arrays, as with crystalline materials, is one of the most significant challenges in the research field as polymorphic arrangements always provide a potential barrier to the preparation of well-defined, ordered arrays. De Feyter et al. approached the question of polymorph screening by designing a mechanism to induce a solution flow across a substrate surface to generate a lateral concentration gradient. This *in situ* generation of a gradient allows both discovery and separation of multiple polymorphs in a single experiment. The authors describe three separate systems: hexadecyloxy-substituted dehydrobenzo[12]-annulene (DBA-OC16), hexadecyl-substituted bis(dehydrobenzo[12]annulene) (bisDBA-C16), and 1,3,5-tris(4-carboxyphenyl)benzene (BTB). Their approach demonstrates systems that exploit either van der Waals or hydrogen-bonding interactions. For each example, more than one polymorph was found for each system by STM imaging of the respective samples; DBA-OC16—two polymorphs; bisDBA-C16—four polymorphs; BTB—two polymorphs (Fig. 12). The approach allows not only structural characterization of the polymorphs observed, but also quantification of surface coverage of each arrangement, giving an approximate yield of the respective polymorphic systems.

2.09.4 Covalently Coupled Two-Dimensional Arrays: Planar Covalent Organic Frameworks

The reversible formation, and hence possible structure correction of both hydrogen bonding and van der Waals interactions allows the formation of well-ordered structures. However, to create robust two-dimensional structures, covalently-bonded frameworks are a more attractive approach. Thus, a strategy that slows the formation of covalently coupled arrays is desirable. A number of approaches have been used to target such systems, including aryl–aryl coupling^{74–77} and alkyne–alkyne coupling⁷⁸ processes. Other approaches have been taken into consideration in recent studies⁷⁹ and the field has clear parallels to studies of covalent organic frameworks or COFs.⁸⁰

An early approach to the development of covalently coupled arrays was the use of the intermolecular coupling between halo-aryl species on Au substrates. Grill et al. developed their approach through the use of porphyrin building blocks with bromophenyl “arms” that protrude from the meso-positions of the porphyrin.⁷⁴ The number of bromophenyl arms can be varied such that a range of building blocks with one, two, or four reactive appendages can be utilized. Reaction of mono-bromophenyl-substituted porphyrin, by heating the building blocks on a Au(111) substrate, leads to dimer formation (Fig. 13A); *trans*-di-bromophenyl-substituted porphyrin reacts to give chains (Fig. 13B) and tetra-bromophenyl-substituted porphyrin can react in all four positions to give well-ordered two-dimensional grids of porphyrins (Fig. 13C). The approach was developed by Grill, Hecht, and coworkers through the construction of covalently coupled arrays built from two different molecular components. Their strategy exploits the difference in reactivity between bromophenyl and iodophenyl groups attached to a porphyrin core in a trans-arrangement leading to different reactivity between the different edges of the porphyrins.^{75,76} Deposition of the dibromo-diiodo-porphyrin ($\text{Br}_2\text{I}_2\text{TPP}$) building block onto a Au(111) substrate and heating the sample results in the covalent coupling between adjacent porphyrin species via the iodo-functionalized edges. This is due to the lower bond dissociation energy of the C–I bonds in comparison to C–Br bonds. Preferential coupling of the two trans-arranged edges leads to the formation of one-dimensional chains of coupled porphyrin building blocks (Fig. 14). Below 200°C only the iodo-functionalized arms react and leave the bromo substituents intact, allowing the possibility of further reaction. However, following the formation of the one-dimensional chains of coupled porphyrins, functionalized with bromophenyl appendages, the reaction with a secondary species can be successfully achieved, as

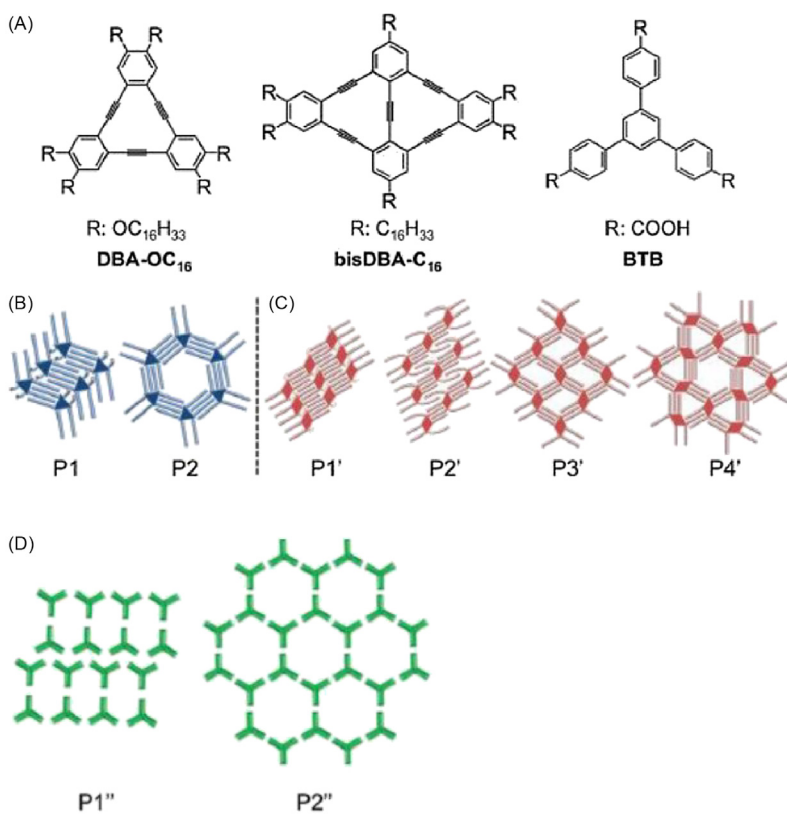


Figure 12 (A) Molecular structures of DBA-OC₁₆, bisDBA-C₁₆, and BTB and representations of the polymorphs observed for each compound (B) DBA-OC₁₆; (C) bisDBA-C₁₆; (D) BTB.⁵⁹ Reproduced with permission from the Royal Society of Chemistry.

demonstrated via codeposition of dibromoterfluorene. Coupling of the bromo-appendages on the porphyrin chain and the terfluorene molecules leads to decoration of the porphyrin chains with terfluorene groups. In some instances, cross-linking of adjacent porphyrin chains is observed and a complex of two-dimensional array of coupled porphyrin chains and terfluorene moieties is formed (Fig. 14). The simple strategy of hierarchical coupling, exploiting dissimilar chemical reactivity and thermal activation barriers for the reactive components, causes the formation of a bimolecular array and opens up the possibility for the creation of more complex covalently coupled arrays.

The strength of the strategy of using covalent coupling to form surface-based arrays is demonstrated by a recent study by Amabilino and Raval.⁸¹ The study reports the coupling of polyaromatic molecules (pentacene, tetramesitylporphyrin, perylene) and porphyrins (H₂-porphyrin and Zn(II)diphenylporphyrin) through C–H bond activation reactions on a copper surface. It is demonstrated that all of the molecules are capable of undergoing C–H activation and can be coupled on the chosen surface. The study demonstrated not only the ability to homo-couple the molecules into extended arrays, for example, Zn(II)diphenylporphyrin can be cross-coupled through the unsubstituted edges (i.e., those not functionalized by phenyl groups) to afford covalently coupled one-dimensional chains of porphyrins, but also the hetero-coupling between the different building blocks. A large variety of coupled structures are described (Fig. 15) with up to three different building blocks cross-coupled. STM studies provide sufficient insight to allow characterization of each individual component of the covalently coupled structure. A related study forms one-dimensional ladders using cross-coupled arrays of Co(II)diphenylporphyrin.⁸² Coadsorption of 1,3-phenylenebis(methylene)-bis-imidazole allows coordination of the imidazole groups to the porphyrin-bound cobalt cation. As a result of the formation of the Co–imidazole bond being reversibly formed it is possible to image the bis-imidazole molecule moving, or walking, from one porphyrin to another along the covalently coupled chains.

These studies demonstrate the ability to prepare highly complex covalently coupled structures from multiple building blocks and indicates the potential for creating bespoke covalent structures on surfaces.

2.09.5 Complex Structures With Low Degrees of Symmetry

One of the features that separates the study of surface-based supramolecular arrays from other areas of supramolecular chemistry is the ability to image the resulting structures at the molecular and submolecular^{18,24} level. This allows a level of detailed

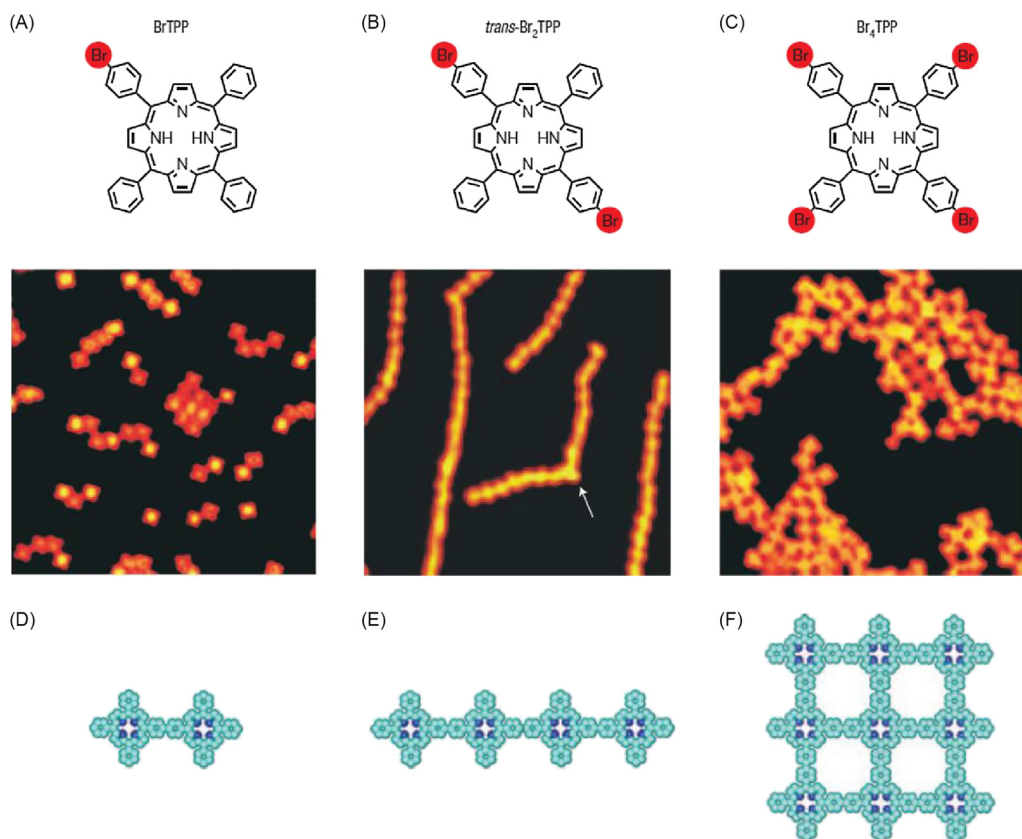


Figure 13 (A–C) Bromophenyl functionalized porphyrin building blocks with increasing numbers of functional moieties for subsequent polymerization. STM images and representative models of (D) dimers prepared from mono-bromophenyl functionalized building-block BrTPP; (E) one-dimensional chains prepared from *trans*-Br₂TPP. The arrow indicates where two chains are held together by weak noncovalent interactions; (F) two-dimensional sheets prepared from covalently coupled Br₄TPP.⁷⁴ Reproduced with permission from the Nature Publishing Group.

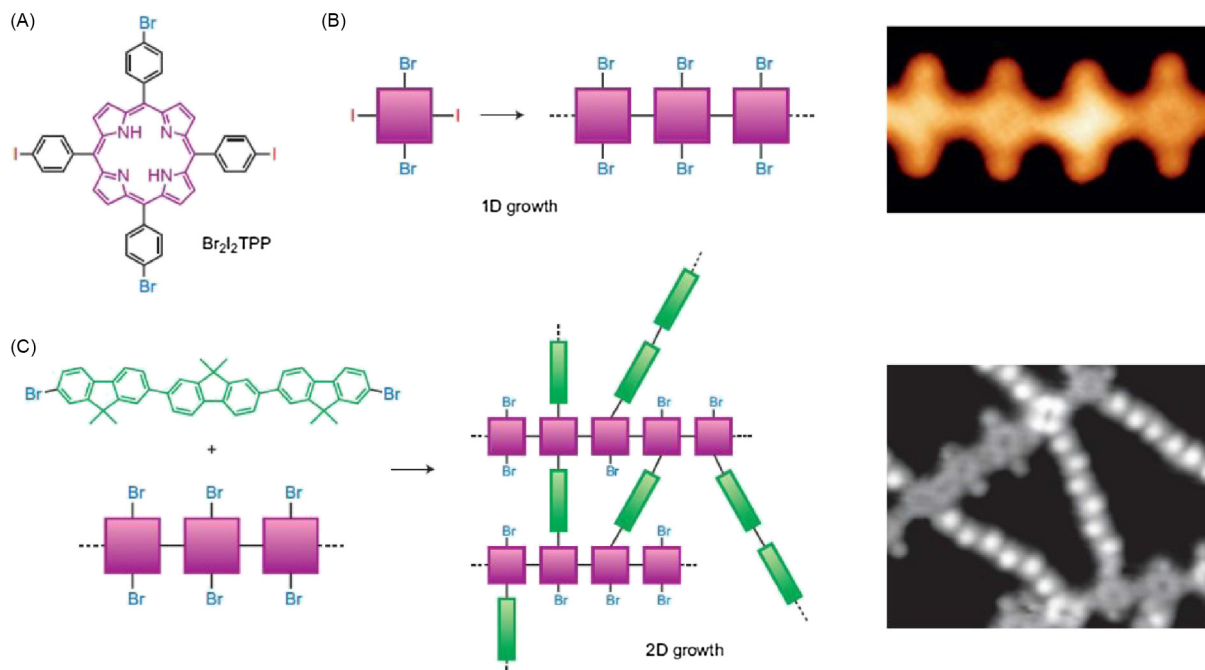


Figure 14 (A) A porphyrin building block with two bromophenyl and two iodophenyl appendages in a trans-arrangement. (B) Aryl-aryl coupling leads to the formation of one-dimensional chains. (C) Subsequent reaction with dibromotetraphluorene leads to the formation of a mixed, covalently coupled framework structure. The STM images confirm the molecular arrangement within the covalently coupled structure.⁷⁶ Reproduced with permission from the Nature Publishing Group.

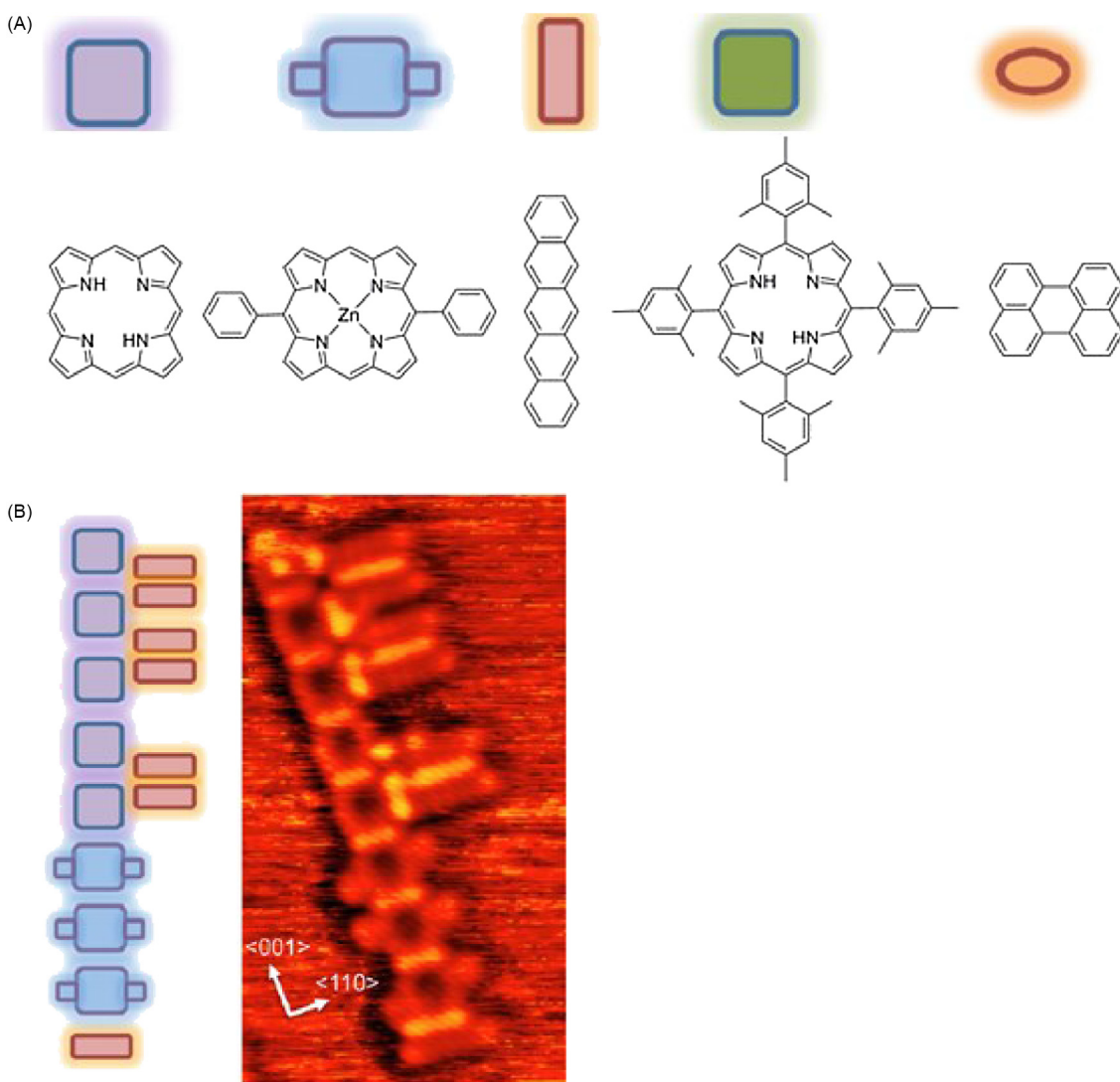


Figure 15 (A) Building blocks capable of undergoing C–H activation on a Cu(110) surface and (B) STM image demonstrating the covalent coupling of three distinct components.⁸¹ Reproduced with permission from the American Chemical Society.

understanding that is extremely challenging, if not impossible, in other areas of supramolecular chemistry due to the methods of characterization employed. The additional level of detail that can be achieved using STM, or AFM, has allowed characterization of structures that would prove extremely challenging by any other technique.

One of the first examples of such a structure is that formed by terphenyl-3,3'',5,5''-tetracarboxylic acid.⁸³ Terphenyl-3,3'',5,5''-tetracarboxylic acid, adsorbed onto HOPG, leads to the formation of a two-dimensional hydrogen-bonded structure that utilizes R₂(8) intermolecular carboxylic acid:carboxylic acid interactions. STM imaging allows identification of the position of each molecule in the framework and direct visualization of a nonordered structure. Indeed, the relative position of molecules within the array is random and reminiscent of dynamically arrested systems such as glasses (Fig. 16). Intermolecular hydrogen bonding leads to the formation of hexagonal junctions which are formed from three, four, five, or six molecules as a result of the dimensions of the molecule. Consequently, the structure forms an extremely rare example of a random, entropically stabilized, rhombus tiling. It is important to note that the detailed structure of this framework, and other related frameworks, can only be appreciated with a molecular level understanding and that this can only be readily achieved by scanning probe microscopies. The degree of randomness of the rhombus tiling can be evaluated by detailed analysis of each image and subsequent studies demonstrated that both solvent used for deposition and temperature of experiment can affect how random the tiling structure is.^{84,85} It is important to note that the rhombus tiling arrangement is only observed for molecules which have the appropriate dimensions, that is, those which are rhombus shaped, and analogous molecules, such as quaterphenyl-3,3'',5,5''-tetracarboxylic acid, form regular two-dimensional structures.⁸⁶

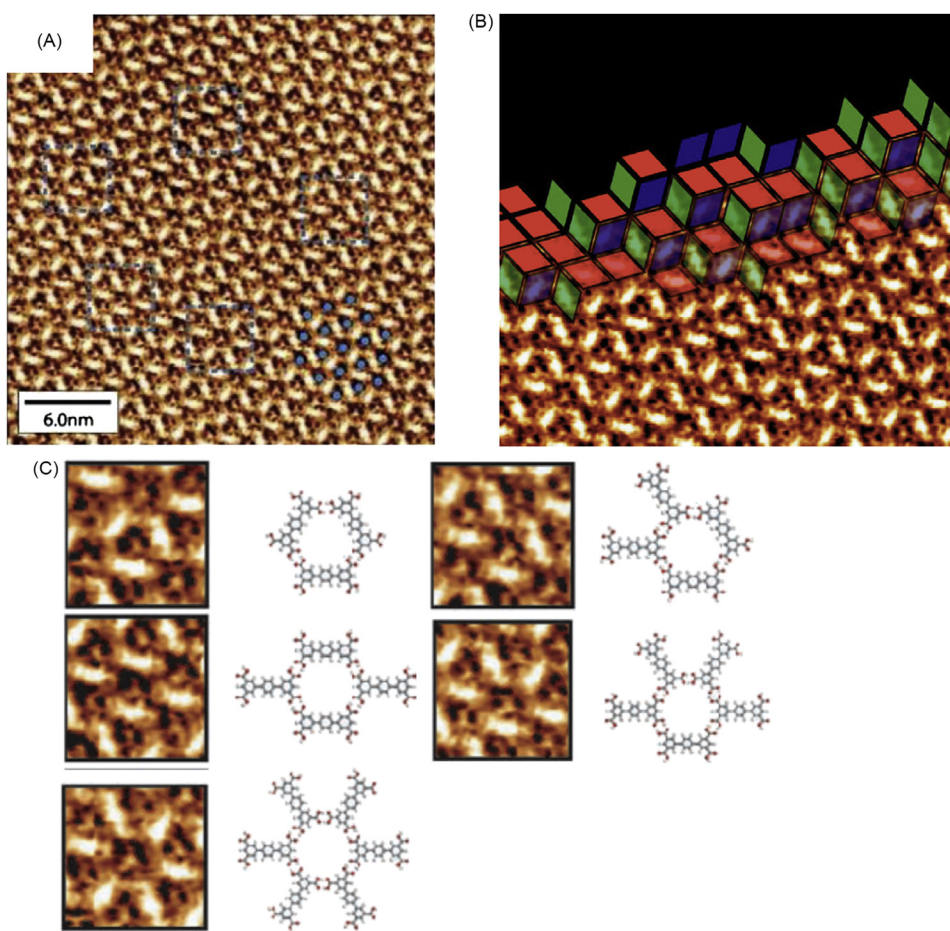


Figure 16 (A) STM image of a typical area of terphenyl-3,3'',5,5''-tetracarboxylic acid network at the nonanoic acid/HOPG interface. The group of three phenyl rings of the molecule backbone appear as *bright features* in the image. The hexagonal orientational order of the structure is indicated by the group of *blue dots* in the *lower right-hand corner* of the image, marking the location of pores in the network. (B) Illustration of how the molecular arrangement, and each molecule, maps onto a rhombus tiling. (C) Diagrams representing the five possible arrangements of terphenyl-3,3'',5,5''-tetracarboxylic acid molecules around a network pore, accompanied by magnified STM image examples of each pore type. The locations of the magnified regions are marked (A) by *blue dashed squares*.⁸³ Reproduced with permission from the AAAS.

The rhombus tiling observed with terphenyl-3,3'',5,5''-tetracarboxylic acid is related to a Penrose tiling⁸⁷; however, the first observation of a structure more closely related to such a tiling structure was reported for the self-assembled supramolecular structure formed by ferrocenecarboxylic acid [Fc(COOH)] on a Au(111) substrate.⁸⁸ Penrose tilings are related to quasicrystal structures in that they exhibit long range, nonperiodic order, and unusual rotational symmetry. Fc(COOH) assembles through intermolecular hydrogen bonding to form pentagonal arrangements of molecules (Fig. 17) with carboxylic acid:carboxylic acid O—H···O interactions being additionally stabilized by C—H···O hydrogen bonds between adjacent molecules. Importantly the cyclic pentamer observed for the surface-based array was found to be more stable than other potential hydrogen-bonding arrangements, such as dimeric systems, by Density Functional Theory (DFT) calculations. It was found that a related compound ferroceneacetic acid [Fc(CH₂COOH)] does not form the pentagonal arrangements, adopting a more conventional dimeric arrangement. This can be accounted for by the observation that the length of the additional methylene group, in comparison to Fc(COOH), prevents interactions between the carboxyl oxygen atom of one carboxylic acid and the hydrogen atoms on an adjacent cyclopentadienyl fragment. The pentagonal arrangements observed are related to subunits of the Penrose P1 tiling.⁸⁷

The search for quasicrystalline structures using molecules has also led to the discovery of a two-dimensional framework built from Europium centers linked through metal-ligand coordination bonds to the bridging ligand *para*-quaterphenyl-dicarbonitrile linker *p*-NC-Ph₄-*p*-CN.⁸⁹ Self-assembly on a Au(111) substrate followed by STM imaging reveals the formation of a quasicrystalline two-dimensional structure. It is clear from the observed structure that due to a combination of fourfold, fivefold, and sixfold coordination of the Eu centers, a structure is formed which represents an irregular tiling of both *triangles* and *squares* (Fig. 18).

Finally, a highly unusual surface-based structure has been reported for the angular molecules 4,4-dibromo-1,1:3,1-terphenyl (B3PB) and 4,4-dibromo-1,1:3,1:4,1-quaterphenyl (B4PB).⁹⁰ Both B3PB and B4PB are functionalized on their termini with bromo-aryl moieties which are instrumental in forming intermolecular halogen bonding interactions (Fig. 19). These interactions

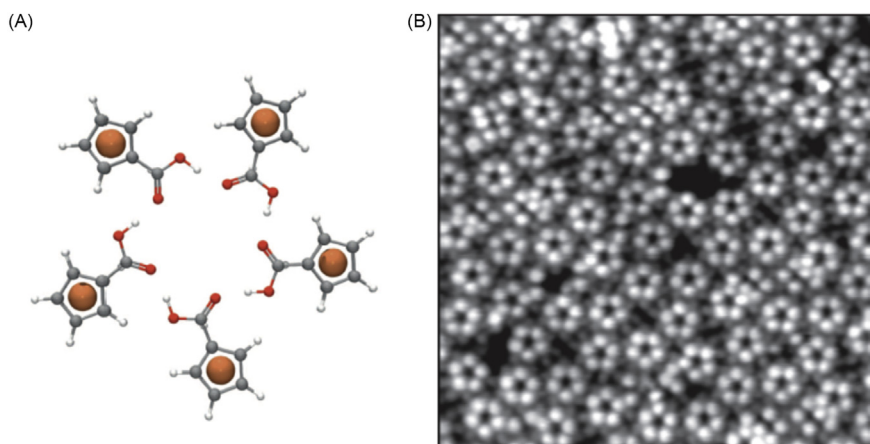


Figure 17 (A) Schematic representation of the pentagonal arrangement formed by $\text{Fc}(\text{COOH})$ through intermolecular hydrogen bonding; (B) pentagonal arrangements can be clearly seen in STM images of $\text{Fc}(\text{COOH})$ adsorbed on a $\text{Au}(111)$ substrate.⁸⁸ Reproduced with permission from the Nature Publishing Group.

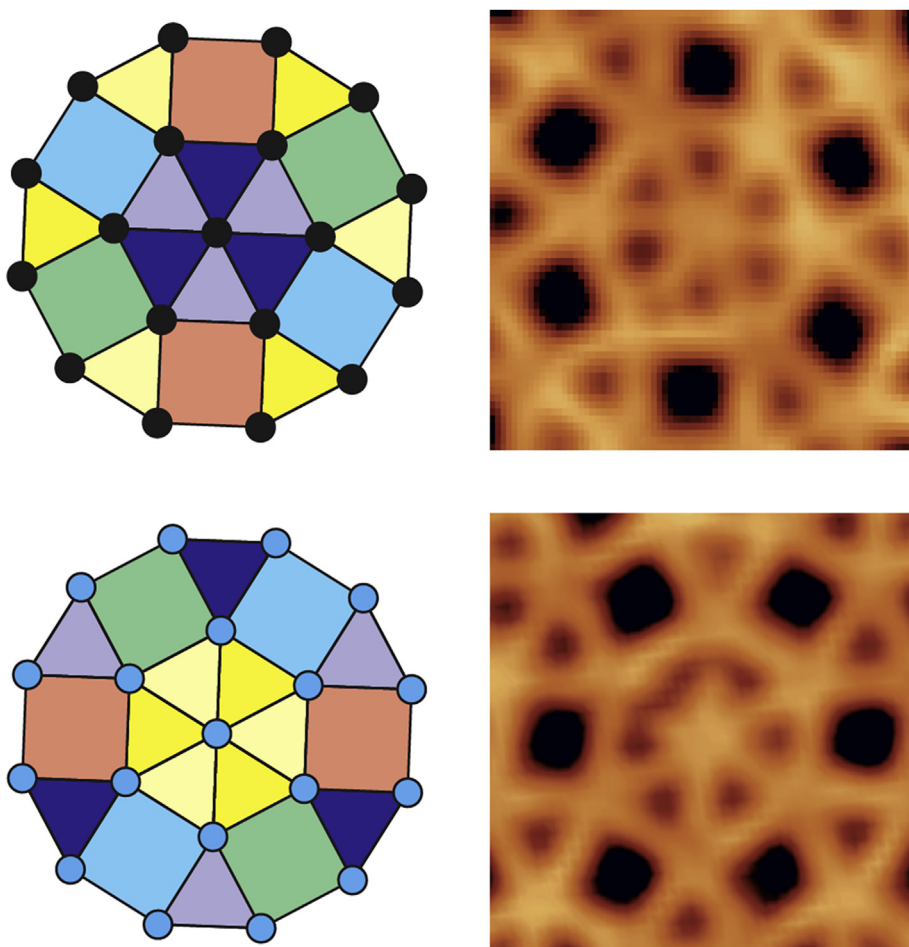


Figure 18 Dodecagonal motifs observed in the quasicrystalline structure formed by $p\text{-NC-Ph}_4\text{-}p\text{-CN}$ and Eu centers on a $\text{Au}(111)$ substrate.⁸⁹ Both triangles and squares can be readily identified, the *different colors* showing the alternative arrangements and orientations of these features with respect to the underlying surface. Reproduced with permission from the Nature Publishing Group.

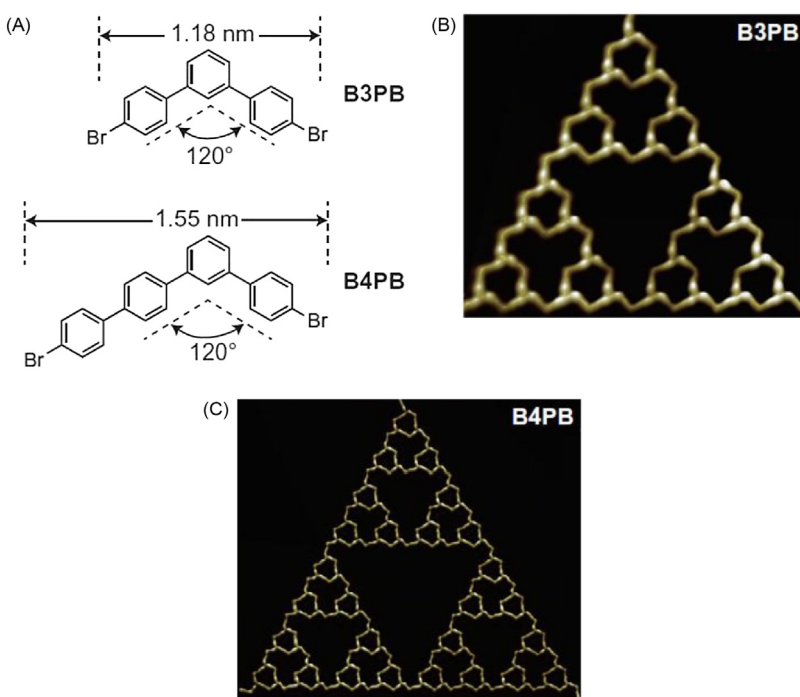


Figure 19 (A) Molecular structures of B3PB and B4PB with dimensions. (B) High resolution STM images of B3PB (13×11 nm) and (C) B4PB (33×29 nm) illustrating the formation of Serpinski triangles by self-assembly of the molecules through halogen bonding.⁹⁰ Reproduced with permission from the Nature Publishing Group.

result in the formation of extended structures which share the same topological arrangement as Serpinski triangles which are fractal structures. The formation of the fractal arrangements is truly remarkable and it is clear that the energy balance between such unusual structures and other potential arrangements is very finely balanced. As with the rhombus and Penrose tilings, it is important to note that a complete appreciation of the structures formed is only possible due to a molecular level understanding of the self-assembled arrangement. This can only be readily achieved using scanning probe microscopies and it is perhaps for this reason that such structures are found in a surface supramolecular frameworks.

2.09.6 Conclusions

It can be clearly seen from the systems described above that surface-based supramolecular chemistry has a rich future building upon an understanding of the interplay between different intermolecular forces and through adsorbate–substrate interactions. The ability to create well-ordered, two-dimensional frameworks shows great promise for the development of bespoke materials. Thus far hydrogen-bonded frameworks have received a great deal of attention, as have those structures that rely on van der Waals interactions to control framework formation, but increasingly the principles of two-dimensional framework formation are being applied to covalently bonded structures. Traditional host–guest chemistry is also feasible using surface-based frameworks opening up strategies of research for the preparation of nanoscale devices.

Although many of the approaches that are employed by supramolecular chemists in either the solution phase or solid state are generally applicable to surface-based processes, significant differences are also evident. Notably, the surface does not play a passive role in the two-dimensional self-assembly process. For molecules to adsorb on the surface there is inherently an interaction between substrate and the molecule and this can lead to subtle differences even affecting the conformations of molecules⁹¹ and the way in which they self-assemble. As the area of surface-based self-assembled frameworks continues to develop, it is important that the role of the substrate becomes increasingly understood and ultimately exploited to control self-assembly. In no area is this more important than in the formation of covalently bonded surface frameworks for which the substrate often plays an integral role in the formation of the covalent bond.

This article demonstrates that a number of successful strategies have already been developed for the synthesis of surface-based framework structures and some of these approaches have led to the discovery of highly unusual structures based upon unusual tiling processes, frameworks which are unlikely to be discovered using other approaches to supramolecular chemistry. Although it is clear that further reliable pathways to robust frameworks still need to be developed, it is also clear that significant progress has already been made in the field. Now that significant success in synthetic strategies has been achieved, the first few steps towards functional materials are already underway.

References

1. Lehn, J. M. *Proc. Natl. Acad. Sci. USA* **2002**, *99*, 4763.
2. Reinhoudt, D. N.; Crego-Calama, M. *Science* **2002**, *295*, 2403.
3. Aakeröy, C.; Champness, N. R.; Janiak, C. *CrystEngComm* **2010**, *12*, 22.
4. Bartels, L. *Nat. Chem.* **2010**, *2*, 87.
5. Bonifazi, D.; Mohnani, S.; Llanes-Pallas, A. *Chem. Eur. J.* **2009**, *15*, 7004.
6. Plass, K. E.; Grzesiak, A. L.; Matzger, A. J. *Acc. Chem. Res.* **2007**, *40*, 287.
7. De Feyter, S.; Gesquière, A.; Abdel-Mottaleb, M. M.; Grim, P. C. M.; De Schryver, F. C. *Acc. Chem. Res.* **2000**, *33*, 520.
8. De Feyter, S.; De Schryver, F. C. *Chem. Soc. Rev.* **2003**, *32*, 139.
9. Kudernac, T.; Lei, S.; Elemans, J. A. A. W.; De Feyter, S. *Chem. Soc. Rev.* **2009**, *38*, 402.
10. Slater (née Phillips), A. G.; Beton, P. H.; Champness, N. R. *Chem. Sci.* **2011**, *2*, 1440–1448.
11. Vericat, C.; Vela, M. E.; Benítez, G.; Carro, P.; Salvarezza, R. C. *Chem. Soc. Rev.* **2010**, *39*, 1805.
12. Narasimhan, S.; Vanderbilt, D. *Phys. Rev. Lett.* **1992**, *69*, 1564.
13. Upward, M. D.; Moriarty, P.; Beton, P. H. *Phys. Rev. B* **1997**, *56*, R1704.
14. Ruben, M.; Lehn, J. M.; Muller, P. *Chem. Soc. Rev.* **2006**, *35*, 1056.
15. Coraux, J.; N'Diaye, A. T.; Busse, C.; Michely, T. *Nano Lett.* **2008**, *8*, 565; Sutter, P. W.; Flege, J.-I.; Sutter, E. A. *Nat. Mater.* **2008**, *7*, 406.
16. Berner, S.; Corso, M.; Widmer, R.; Groening, O.; Laskowski, R.; Blaha, P.; Schwarz, K.; Goriachko, A.; Over, H.; Gsell, S.; Schreck, M.; Sachdev, H.; Greber, T.; Osterwalder, J. *Angew. Chem. Int. Ed.* **2007**, *46*, 5115.
17. Korolkov, V. V.; Svatek, S. A.; Allen, S.; Roberts, C. J.; Tendler, S. J. B.; Taniguchi, T.; Watanabe, K.; Champness, N. R.; Beton, P. H. *Chem. Commun.* **2014**, *50*, 8882–8885.
18. Gross, L.; Mohn, F.; Moll, N.; Liljeroth, P.; Meyer, G. *Science* **2009**, *325*, 1110–1114.
19. Whitesides, G. M.; Simanek, E. E.; Mathias, J. P.; Seto, C. T.; Chin, D. N.; Mammen, M.; Gordon, D. M. *Acc. Chem. Res.* **1995**, *28*, 37.
20. Griessl, S.; Lackinger, M.; Edelwirth, M.; Hietzschold, M.; Heckl, W. M. *Single Mol.* **2002**, *3*, 25.
21. Etter, M. C. *Acc. Chem. Res.* **1990**, *23*, 120–126.
22. Gutzler, R.; Sirtl, T.; Dienstmaier, J. F.; Mahata, K.; Heckl, W. M.; Schmittel, M.; Lackinger, M. *J. Am. Chem. Soc.* **2010**, *132*, 5084.
23. Keeling, D. L.; Oxtoby, N. S.; Wilson, C.; Humphry, M. J.; Champness, N. R.; Beton, P. H. *Nano Lett.* **2003**, *3*, 9.
24. Sweetman, A. M.; Jarvis, S.; Sang, H.; Lekkas, I.; Rahe, P.; Wang, Y.; Wang, J.; Champness, N. R.; Kantorovich, L.; Moriarty, P. *Nat. Commun.* **2014**, *5*, 3931.
25. Sweetman, A. M.; Jarvis, S. P.; Champness, N. R.; Rahe, P.; Kantorovich, L.; Moriarty, P. *Phys. Rev. B* **2014**, *90*, 165425.
26. Jarvis, S. P.; Sweetman, A. M.; Lekkas, I.; Champness, N. R.; Kantorovich, L.; Moriarty, P. *J. Phys. Condens. Matter* **2015**, *27*, 054004.
27. Jarvis, S. P.; Rashid, M. A.; Sweetman, A.; Leaf, J.; Taylor, S.; Moriarty, P.; Dunn, J. *Phys. Rev. B* **2015**, *92*, 241405.
28. Seeman, N. C. *Nature* **2003**, *421*, 427.
29. Edwardson, T. G. W.; Lau, K. L.; Bousmail, D.; Sleiman, H. *Nat. Chem.* **2016**, *8*, 162–170; Mirkin, C. A.; Letsinger, R. L.; Mucic, R. C.; Storhoff, J. J. *Nature* **1996**, *382*, 607–609.
30. Winfree, E.; Liu, F.; Wenzler, L. A.; Seeman, N. C. *Nature* **1998**, *394*, 539.
31. He, Y.; Chen, Y.; Liu, H.; Ribbe, A. E.; Mao, C. *J. Am. Chem. Soc.* **2005**, *127*, 12202.
32. Otero, R.; Schock, M.; Molina, L. M.; Laegsgaard, E.; Stensgaard, I.; Hammer, B.; Besenbacher, F. *Angew. Chem. Int. Ed.* **2005**, *44*, 2270.
33. Ciesielski, A.; Perone, R.; Pieraccini, S.; Piero Spada, G.; Samori, P. *Chem. Commun.* **2010**, *46*, 4493.
34. Ciesielski, A.; Haar, S.; El Garah, M.; Surin, M.; Masiero, S.; Samori, P. *L'Actual. Chim.* **2015**, *399*, 31–36.
35. El Garah, M.; Perone, R. C.; Santana Bonilla, A.; Haar, S.; Campitiello, M.; Gutierrez, R.; Cuniberti, G.; Masiero, S.; Ciesielski, A.; Samori, P. *Chem. Commun.* **2015**, *51*, 11677–11680.
36. Ciesielski, A.; El Garah, M.; Masiero, S.; Samori, P. *Small* **2016**, *12*, 83–95.
37. Slater, A. G.; Hu, Y.; Yang, L.; Argent, S. P.; Lewis, W.; Blunt, M. O.; Champness, N. R. *Chem. Sci.* **2015**, *6*, 1562–1569.
38. Elemans, J. A. A. W.; De Cat, I.; Xu, H.; De Feyter, S. *Chem. Soc. Rev.* **2009**, *38*, 722–736.
39. Bilbao, N.; Destoop, I.; De Feyter, S.; González-Rodríguez, D. *Angew. Chem. Int. Ed.* **2016**, *55*, 659–663.
40. Zerkowski, J. A.; Mathias, J. P.; Whitesides, G. M. *J. Am. Chem. Soc.* **1994**, *116*, 4305.
41. Slater, A. G.; Perdigão, L. M. A.; Beton, P. H.; Champness, N. R. *Acc. Chem. Res.* **2014**, *47*, 3417–3427.
42. Theobald, J. A.; Oxtoby, N. S.; Phillips, M. A.; Champness, N. R.; Beton, P. H. *Nature* **2003**, *424*, 1029–1031.
43. Theobald, J. A.; Oxtoby, N. S.; Champness, N. R.; Beton, P. H.; Dennis, T. J. S. *Langmuir* **2005**, *21*, 2038.
44. Silly, F.; Shaw, A. Q.; Porfyrikis, K.; Warner, J. H.; Watt, A. A. R.; Castell, M. R.; Umemoto, H.; Akachi, T.; Shinohara, H.; Briggs, G. A. D. *Chem. Commun.* **2008**, 4616.
45. Perdigão, L. M. A.; Perkins, E. W.; Ma, J.; Stanić, P. A.; Rogers, B. L.; Champness, N. R.; Beton, P. H. *J. Phys. Chem. B* **2006**, *110*, 12539.
46. Stanić, P. A.; Perdigão, L. M. A.; Saywell, A.; Champness, N. R.; Beton, P. H. *ChemPhysChem* **2007**, *8*, 2177.
47. Perdigão, L. M. A.; Stanić, P. A.; Champness, N. R.; Beton, P. H. *Langmuir* **2009**, *25*, 2278.
48. Madueno, R.; Räisänen, M. T.; Silien, C.; Buck, M. *Nature* **2008**, *454*, 618.
49. Silien, C.; Räisänen, M. T.; Buck, M. *Small* **2010**, *6*, 391.
50. Silien, C.; Räisänen, M. T.; Buck, M. *Angew. Chem. Int. Ed.* **2009**, *48*, 3349.
51. Lombana, A.; Battaglini, N.; Tsague-Kenfac, G.; Zrig, S.; Lang, P. *Chem. Commun.* **2016**, *52*, 5742–5745.
52. Lombana, A.; Rinfray, C.; Volatron, F.; Izett, G.; Battaglini, N.; Alves, S.; Decorse, P.; Lang, P.; Proust, A. *J. Phys. Chem. C* **2016**, *120*, 2837–2845.
53. Saywell, A.; Magnano, G.; Satterley, C. J.; Perdigão, L. M. A.; Champness, N. R.; Beton, P. H.; O'Shea, J. N. *J. Phys. Chem. C* **2008**, *112*, 7706–7709.
54. Saywell, A.; Magnano, G.; Satterley, C. J.; Perdigão, L. M. A.; Britton, A. J.; Taleb, N.; Giménez-López, M. C.; Champness, N. R.; O'Shea, J. N.; Beton, P. H. *Nat. Commun.* **2010**, *1*, 75.
55. Pollard, A. J.; Perkins, E. W.; Smith, N. A.; Saywell, A.; Goretzki, G.; Phillips, A. G.; Argent, S. P.; Sachdev, H.; Müller, F.; Hüfner, S.; Gsell, S.; Fischer, M.; Schreck, M.; Osterwalder, J.; Greber, T.; Berner, S.; Champness, N. R.; Beton, P. H. *Angew. Chem. Int. Ed.* **2010**, *49*, 1794–1799.
56. Perdigão, L. M. A.; Saywell, A.; Fontes, G. N.; Stanić, P. A.; Goretzki, G.; Phillips, A. G.; Champness, N. R.; Beton, P. H. *Chem. Eur. J.* **2008**, *14*, 7600.
57. Räisänen, M. T.; Slater (née Phillips), A. G.; Champness, N. R.; Buck, M. *Chem. Sci.* **2012**, *3*, 84–92.
58. Phillips, A. G.; Perdigão, L. M. A.; Beton, P. H.; Champness, N. R. *Chem. Commun.* **2010**, *46*, 2775.
59. Lee, S.-L.; Adisojojo, J.; Fang, Y.; Tahara, K.; Tobe, Y.; Mali, K. S.; De Feyter, S. *Nanoscale* **2015**, *7*, 5344–5349.
60. Berdunov, N.; Pollard, A. J.; Beton, P. H. *Appl. Phys. Lett.* **2009**, *94*, 043110.
61. Perdigão, L. M. A.; Champness, N. R.; Beton, P. H. *Chem. Commun.* **2006**, *5*, 538.
62. Stanić, P. A.; Perdigão, L. M. A.; Rogers, B. L.; Champness, N. R.; Beton, P. H. *J. Phys. Chem. C* **2007**, *111*, 886–893.
63. Palma, C.-A.; Bjork, J.; Bonini, M.; Dyer, M. S.; Llanes-Pallas, A.; Bonifazi, D.; Persson, M.; Samori, P. *J. Am. Chem. Soc.* **2009**, *131*, 13062.
64. Wieghold, S.; Li, J.; Simon, P.; Krause, M.; Avlasevich, Y.; Li, C.; Garrido, J. A.; Heiz, U.; Samori, P.; Mullen, K.; Esch, F.; Barth, J. V.; Palma, C.-A. *Nat. Commun.* **2016**, *7*, 10700.

65. Mali, K. S.; Adisoejoso, J.; Ghijssens, E.; De Cat, I.; De Feyter, S. *Acc. Chem. Res.* **2012**, *45*, 1309–1320.
66. Mali, K. S.; De Feyter, S. *Phil. Trans. R. Soc. A* **2013**, *371*, 20120304.
67. Schull, G.; Douillard, L.; Florini-Debuisschert, C.; Charra, F. *Nano Lett.* **2006**, *6*, 1360.
68. Tahara, K.; Okuhata, S.; Adisoejoso, J.; Lei, S.; Fujita, T.; De Feyter, S.; Tobe, Y. *J. Am. Chem. Soc.* **2009**, *131*, 17583.
69. Elemans, J. A. A. W.; Lei, S. B.; De Feyter, S. *Angew. Chem. Int. Ed.* **2009**, *48*, 7298.
70. Lei, S.; Surin, M.; Tahara, K.; Adisoejoso, J.; Lazzaroni, R.; Tobe, Y.; De Feyter, S. *Nano Lett.* **2008**, *8*, 2541.
71. Lei, S.; Tahara, K.; De Schryver, F. C.; Van der Auweraer, M.; Tobe, Y.; De Feyter, S. *Angew. Chem. Int. Ed.* **2008**, *47*, 2964.
72. Furukawa, S.; Uji-i, H.; Tahara, K.; Ichikawa, T.; Sonoda, M.; De Schryver, F. C.; Tobe, Y.; De Feyter, S. *J. Am. Chem. Soc.* **2006**, *128*, 3502.
73. Tahara, K.; Furukawa, S.; Uji-i, H.; Uchino, T.; Ichikawa, T.; Zhang, J.; Sonoda, M.; De Schryver, F. C.; De Feyter, S.; Tobe, Y. *J. Am. Chem. Soc.* **2006**, *128*, 16613.
74. Grill, L.; Dyer, M.; Lafferentz, L.; Persson, M.; Peters, M. V.; Hecht, S. *Nat. Nanotechnol.* **2007**, *2*, 687.
75. Lafferentz, L.; Eberhardt, V.; Dri, C.; Africh, C.; Comelli, G.; Esch, F.; Hecht, S.; Grill, L. *Nat. Chem.* **2012**, *4*, 215–220.
76. Champness, N. R. *Nat. Chem.* **2012**, *4*, 149–150.
77. Blunt, M. O.; Russell, J. C.; Champness, N. R.; Beton, P. H. *Chem. Commun.* **2010**, *46*, 7157–7159.
78. Klappenberger, F.; Zhang, Y.-Q.; Bjork, J.; Klyatskaya, S.; Ruben, M.; Barth, J. V. *Acc. Chem. Res.* **2015**, *48*, 2140–2150.
79. Clair, S.; Abel, M.; Porte, L. *Chem. Commun.* **2014**, *50*, 9627–9635.
80. Ding, S.-Y.; Wang, W. *Chem. Soc. Rev.* **2013**, *42*, 548–568.
81. Haq, S.; Hanke, F.; Sharp, J.; Persson, M.; Amabilino, D. B.; Raval, R. *ACS Nano* **2014**, *8*, 8856–8870.
82. Haq, S.; Wit, B.; Sang, H.; Floris, A.; Wang, Y.; Wang, J.; Perez-Garcia, L.; Kantorovitch, L.; Amabilino, D. B.; Raval, R. *Angew. Chem. Int. Ed.* **2015**, *54*, 7101–7105.
83. Blunt, M. O.; Russell, J.; Giménez-López, M. C.; Garrahan, J. P.; Lin, X.; Schröder, M.; Champness, N. R.; Beton, P. H. *Science* **2008**, *322*, 1077–1081.
84. Stannard, A.; Russell, J. C.; Blunt, M. O.; Sallesiotis, C.; Gimenez-Lopez, M. C.; Taleb, N.; Schröder, M.; Champness, N. R.; Garrahan, J. P.; Beton, P. H. *Nat. Chem.* **2012**, *4*, 112–117.
85. Blunt, M. O.; Russell, J. C.; Gimenez-Lopez, M. C.; Taleb, N.; Lin, X.; Schröder, M.; Champness, N. R.; Beton, P. H. *Nat. Chem.* **2011**, *3*, 74–78.
86. Blunt, M. O.; Lin, X.; Gimenez-Lopez, M. C.; Schröder, M.; Champness, N. R.; Beton, P. H. *Chem. Commun.* **2008**, 2304.
87. Penrose, R. *Eureka* **1978**, *39*, 16–32.
88. Wasio, N. A.; Quardokus, R. C.; Forrest, R. P.; Lent, C. S.; Corcelli, S. A.; Christie, J. A.; Henderson, K. W.; Kandel, S. A. *Nature* **2014**, *507*, 86–89.
89. Urgel, J. I.; Écija, D.; Lyu, G.; Zhang, R.; Palma, C.-A.; Auwärter, W.; Lin, N.; Barth, J. V. *Nat. Chem.* **2016**, *8*, 657–662.
90. Shang, J.; Wang, Y.; Chen, M.; Dai, J.; Zhou, X.; Kuttner, J.; Hilt, G.; Shao, X.; Gottfried, J. M.; Wu, K. *Nat. Chem.* **2015**, *7*, 389–393.
91. Jarvis, S. P.; Taylor, S.; Baran, J. D.; Champness, N. R.; Larsson, J. A.; Moriarty, P. *Nat. Commun.* **2015**, *6*, 8338.